Osmium isotope evidence for a heterogeneous 3He/4He mantle plume beneath the Juan Fernandez Islands

Marine Paquet, James M D Day, Paterno R Castillo

Osmium isotope evidence for a heterogeneous $^{3}He/^{4}He$ mantle plume beneath the Juan Fernandez Islands

Marine Paquet, James M.D. Day, Paterno R. Castillo

Scripps Institution of Oceanography, University of California San Diego, La Jolla, CA 92093, USA. Corresponding author: mpaquet@ucsd.edu

RESEARCH HIGHLIGHTS

- Highly siderophile and trace element abundances in Juan Fernandez lavas controlled by melting and fractional crystallization processes
- Osmium isotopic compositions are unaffected by shallow petrogenetic processes.
- Robinson Crusoe and Alexander Selkirk main shield lavas distinct in He-Sr-Nd-Os-Pb isotope compositions, indicating heterogeneous mantle plume.
- Robinson Crusoe rejuvenated lavas compositions are contaminated by a noble gas impregnated lithospheric mantle.

Keywords: Osmium isotopes; highly siderophile elements; Juan Fernandez; mantle geochemistry; Ocean Island Basalts

ABSTRACT (422 words)

Mantle plume models have been widely applied to explain the formation of ocean island basalts (OIB), with high-$^{3}He/^{4}He$ in their lavas being explained by sampling of a primitive deep mantle source. The Juan Fernandez Islands have $^{3}He/^{4}He$ (7.8-18R_A) similar to or higher than in mid ocean ridge basalts (MORB; 8 ±1 R_A) and have been used to both support and refute the mantle plume hypothesis. Ambiguity regarding the origin of the Juan Fernandez Islands primarily originates from interpretation of mantle source signatures between the lava series from the two main islands, Robinson Crusoe and Alexander Selkirk. To examine this issue, we report new whole-rock and olivine separate $^{187}Os/^{188}Os$ ratios and major-, trace-, and highly siderophile-element (HSE: Re, Pd, Pt, Ru, Ir, Os) abundances. The HSE and trace element abundances in Juan Fernandez main shield lavas can be explained by up to 30% olivine removal, together with spinel crystallization at 1-5 kbar, whereas Robinson Crusoe rejuvenated lavas can be reproduced by higher-pressure fractional crystallization (up to 10 kbar). An assemblage of 30 modal % olivine and 1-5 modal % spinel, combined with the additional contribution of primary melt trapped in olivine inclusions reproduces the range of HSE compositions observed in Juan Fernandez Archipelago olivine grains. Ratios of $^{187}Os/^{188}Os$ for Juan Fernandez lavas are generally less radiogenic than global OIB and show no correlation with indices of fractionation, indicating that they reflect mantle source compositions. Younger basanite lavas from Robinson Crusoe represent rejuvenated volcanism dominantly from a depleted lithospheric mantle source ($^{187}Os/^{188}Os$ <0.13) mixed with a high-$^{3}He/^{4}He$ component from the main shield building stage. These lavas are similar in origin and composition to other Pacific rejuvenated lavas (e.g., Samoa, Hawaii). Robinson Crusoe main shield lavas are from a high-$^{3}He/^{4}He$ (>18R_A) and enriched mantle source ($^{187}Os/^{188}Os$ = 0.1312) similar to the 'C' or 'FOZO' component, whereas Alexander Selkirk lavas are consistent with a dominant contribution from a depleted, low-$^{3}He/^{4}He$ (<10R_A) mantle component. The mantle sources of the shield lavas yield subtle variations in Sr-Nd-Os-Pb isotope space and have no clear variations with relative or absolute abundances of the HSE or trace elements. These results are consistent with a heterogeneous mantle plume model, with initial eruption of lavas from a primitive high-$^{3}He/^{4}He$ mantle source ~4 million years ago (Ma) to form Robinson Crusoe Island, which also led to ^{3}He enrichment of the oceanic lithosphere, followed by eruption of Alexander Selkirk lavas from a more depleted mantle source at ~2 Ma. Juan Fernandez lavas show that mantle heterogeneity preserved in OIB

54 can occur over short-timescales (<2 Ma) and can impact lithospheric compositions, leading to
55 eruption of rejuvenated lavas with unusual isotopic characteristics.
56
57 **1. INTRODUCTION**

58 Ocean island basalts (OIB) with high $^{3}He/^{4}He$ ratios (e.g., Hawaii, Iceland, Galapagos,
59 Samoa, Reunion and the Juan Fernandez Islands) are widely considered to originate from
60 primordial lower mantle via upwelling plumes (e.g. Kurz et al., 1982; Hart et al., 1992; Farley et
61 al., 1992). Hence, these high-$^{3}He/^{4}He$ OIB are probes to better constrain the composition of the
62 deep mantle. High-$^{3}He/^{4}He$ lavas are linked to conventional radiogenic isotope systematics in
63 that they converge to a common mantle component in Sr-Nd-Pb isotope space, variably called
64 FOZO (Focus Zone: Hart et al., 1992), PHEM (Primitive Helium Mantle: Farley et al., 1992), or
65 C (Common: Hanan and Graham, 1996), which only differ in detail from their isotope
66 compositions in Sr, Nd and Pb isotopes, if at all (Hofmann, 2014).
67
68 The Juan Fernandez volcanic chain in the southeastern Pacific is an important location for
69 investigating geochemical variations in OIB in so far as its lavas show a large range of $^{3}He/^{4}He$
70 compositions, between 7.8 to 18.0 R_A ($^{3}He/^{4}He$ normalized to air; Farley et al., 1993), from
71 normal MORB-like ratios (8 ± 1 R_A; Graham, 2002) to higher ratios, which have previously been
72 interpreted as a deep-mantle source signature (e.g. Kurz et al., 1982; Hart et al., 1992). In
73 contrast to their variable He isotope compositions, Juan Fernandez lavas span a limited range of
74 Sr-Nd-Pb isotope ratios (Gerlach et al., 1986; Baker et al., 1987; Farley et al., 1993; Truong et
75 al., 2018). The Juan Fernandez volcanic island and seamount chain is located at 34°S on the
76 Nazca Plate, between 76° and 83°W, approximately 660 km west of Chile (Figure 1). The chain
77 is composed of two main islands, 180 km apart from each other, Robinson Crusoe (also called

Mas a Tierra, closer to the land, at approximately 78°50'W), and Alexander Selkirk (Mas Afuera, away from the land, at approximately 80°50'W). A small island, Santa Clara, to the southwest of Robinson Crusoe, and numerous seamounts rise along the aseismic ridge oriented east-west at 34°S (Baker et al., 1983; Farley et al., 1993; Devey et al., 2000; Rodrigo and Lara, 2014; Lara et al., 2018a, 2018b). Radiometric ($^{40}Ar/^{39}Ar$) ages for shield lavas range between 8.41-9.26 Ma for O'Higgins Guyot (e.g. Lara et al., 2018b), 3.40–4.10 Ma for Robinson Crusoe Island (Reyes et al., 2017; Lara et al., 2018b), and 0.83–0.94 Ma for Alexander Selkirk Island (Lara et al., 2018b). Previous studies reported K-Ar ages up to 5.8 ± 2.1 Ma for Santa Clara, from 3.1 ± 0.9 to 4.2 ± 0.2 Ma for Robinson Crusoe, and from 0.85 ± 0.3 Ma to 2.4 ± 0.1 Ma for Alexander Selkirk (Booker et al., 1967; Stuessy et al., 1984; Baker et al., 1987). All available age data suggest a difference between Robinson Crusoe and Alexander Selkirk Islands of ~2 to 3 Ma, which is in good agreement with the Nazca Plate moving eastward at a spreading rate of about 74 $mm.yr^{-1}$ (DeMets et al., 2010). Previous studies described fresh basalts from Friday and Domingo seamounts (Farley et al., 1993; Devey et al., 2000), indicating that these seamounts are younger than Alexander Selkirk. The progressively younger ages to the west support the hypothesis of an age-progressive hotspot volcanism.

Early studies argued that the eastward movement of the Nazca Plate over a stationary plume formed the Juan Fernandez volcanic chain, making new volcanoes in the west while the magma supply to the older volcanoes was decreasing (Baker et al., 1987; Farley et al., 1993). Farley et al. (1993) proposed that the observed variations in helium isotopic compositions might be attributed to the mixing of the plume component, with a heterogeneous distribution of volatiles or having suffered extraction of small degree partial melts prior to mixing, and an asthenospheric

component. The Juan Fernandez plume is now thought to sample both FOZO and a relatively depleted component (with MORB-like $^{3}He/^{4}He$ ratios) during the shield building stage, whereas the rejuvenated phase of the plume sampled mostly the FOZO component (Truong et al., 2018). These two stages, shield and rejuvenated volcanism in the Juan Fernandez Islands, have contrasting patterns of magma ascent and storage (Reyes et al., 2017) and correspond to a classical example of intraplate magmatism fed by a mantle plume; mechanisms also proposed for other OIB, like Hawaii or Réunion. Conversely, Natland (2003) suggested that the helium contents measured in olivine crystals in Juan Fernandez lavas were indicative of mantle-derived volatiles, not derived from a plume, that pervaded magma conduits and storage reservoirs at shallow levels to be trapped in crystallizing olivine.

Highly siderophile elements (HSE: Os, Ir, Ru, Rh, Pt, Pd, Re and Au) and Os isotopes are potential arbitrators for understanding shallow versus deep mantle processes. In basaltic magmas, the HSE show highly compatible (Os, Ir, Ru), to compatible (Pt and Pd) or moderately incompatible (Re) behavior. These elements typically have parallel liquid lines of descent during fractional crystallization, which are controlled by spinel, olivine or sulfide fractionation (e.g. Puchtel and Humayun, 2001; Ireland et al., 2009; Day, 2013). In particular, the partition coefficient for Ru between spinel and melt is one to two orders of magnitude higher than for the other HSE (e.g. Day, 2013). Therefore, HSE signatures in OIB can be dominated by mantle components, due to the corresponding low abundances of these elements in crustal rocks, but can also record shallow level fractionation processes (Day, 2013). This behavior contrasts with other lithophile isotopic systems (Sr-Nd-Pb-Hf) usually documented in OIB; these elements tend to be

123 enriched in crustal and sedimentary rocks (>>ppm level), which can be assimilated by melts and
124 obscure the isotopic and elemental signature of the mantle source (<ppm level).
125
126 The long-lived ^{187}Re-^{187}Os decay system ($^{187}Re \rightarrow {}^{187}Os + \beta^-$; $\lambda = 1.6668 \times 10^{-11} a^{-1}$; Selby et
127 al., 2007) is an important tool for characterizing the geochemical history of mantle reservoirs.
128 Rhenium and Os have contrasting incompatibilities during melting, with Os being retained
129 within the residue and Re being incompatible, resulting in large isotopic variations generated in
130 crustal reservoirs ($^{187}Os/^{188}Os \geq 1$; e.g. Day, 2013 and references therein), and smaller, generally
131 subchondritic $^{187}Os/^{188}Os$ variations ($^{187}Os/^{188}Os = 0.13$) in peridotites (e.g. Day, 2013 and
132 references therein). Abundances of the HSE, coupled with the long-lived ^{187}Re-^{187}Os decay
133 system, are therefore important tools for characterizing the geochemical history of mantle
134 reservoirs and shallow petrogenetic processes affecting magmas and their volcanic products (e.g.
135 Rehkämper et al., 1997; Brandon & Walker, 2005; Day, 2013).
136
137 We present whole-rock and olivine separate Os isotope compositions and major- (for olivine
138 separates), trace- and highly siderophile-element abundances for "shield stage" alkali basalts and
139 "post-shield stage or rejuvenated" basanites from the two main islands of the Juan Fernandez
140 Archipelago, Robinson Crusoe and Alexander Selkirk that were previously analyzed by Farley et
141 al. (1993) and Truong et al. (2018) (see Table S1 for the compilation of all data available for the
142 Juan Fernandez lavas and olivine grains), as well as *in situ* major and highly siderophile-element
143 compositions of the spinel inclusions identified in the olivine grains. The objectives of this study
144 are: (1) to complement the global OIB dataset with lavas from the Juan Fernandez Islands for
145 HSE abundances and Os isotope compositions and compare them with other primitive plume-

derived lavas from Hawaii, Réunion or Canary Islands, and (2) investigate the origin of the Juan Fernandez Islands, and in particular the differences in mantle source signature for the lava series from Robinson Crusoe and Alexander Selkirk. Combining Os and He isotopes has the potential to better explain the source contributions in Juan Fernandez lavas, and the origin of their variable $^{3}He/^{4}He$ ratios.

2. SAMPLES AND METHODS

The samples examined in this study were collected in 1988, during Leg I of the Scripps Institution of Oceanography Hydros expedition. We analyzed 17 basalts (11 samples from Robinson Crusoe; 6 samples from Alexander Selkirk), as well as olivine separates from three of these samples (two from Robinson Crusoe; one from Alexander Selkirk), for their Os isotope compositions, highly siderophile element (HSE: Re, Pd, Pt, Ru, Ir, Os) and trace element abundances. Samples from Robinson Crusoe include 'main shield' olivine tholeiites and alkali basalts, previously termed Group I lavas by Farley et al. (1993), and younger basanite lavas (termed Group II by Farley et al., 1993) that correspond to the rejuvenated post-shield stages of Robinson Crusoe Island (Reyes et al., 2017; Truong et al., 2018). Samples from Alexander Selkirk comprise mostly olivine tholeiites (termed Group III by Farley et al., 1993), and correspond to the main shield stage during formation of the island (Reyes et al., 2017; Truong et al., 2018).

Whole-rock powders and olivine separates were obtained from the study of Troung et al. (2018). The olivine separates were 100% pure olivine, however, dark inclusions were observed in virtually all olivine grains and could not be removed from the separate due to the requirement

for sufficient analyte for Os isotope and HSE abundance analyses. Osmium isotope and HSE abundance analyses were performed at the Scripps Isotope Geochemistry Laboratory (SIGL). One gram of finely ground and homogenized sample powder was precisely weighed and then digested in sealed 20 cm long borosilicate Carius tubes using a mixture of multiply Teflon distilled HCl (4 mL) and 'purged' HNO_3 (7 mL; expunged of Os using H_2O_2), with isotopically enriched multi-element spikes (^{99}Ru, ^{106}Pd, ^{185}Re, ^{190}Os, ^{191}Ir, ^{194}Pt). Digestions lasted for 72 hours in an oven at a maximum temperature of 240°C.

After digestion, Os was extracted from aqua regia in three steps using CCl_4 and then back-extracted using HBr (Cohen and Water, 1996), before being purified by micro-distillation (Birck et al., 1997). The other HSE (Re, Pd, Pt, Ru, Ir) were recovered and purified from the residual solutions using anion exchange column chemistry (Day et al., 2014, 2016). Osmium isotopic measurements were performed using a *Thermo Scientific Triton* thermal ionization mass spectrometer in negative ion mode, and Re, Pd, Pt, Ru and Ir abundances were measured using a *Thermo Scientific* iCaP Qc ICP-MS coupled to a *Cetac Aridus II* desolvating nebulizer. Osmium isotope and abundance data were appropriately oxide-, fractionation-, spike- and blank corrected (Day et al., 2016). Precision for $^{187}Os/^{188}Os$, determined by repeated measurements of the 35 pg UMCP Johnson-Matthey standard, was better than ± 0.2% (2SD; 0.11357 ± 23; n = 7). Rhenium, Pd, Pt, Ir and Ru isotopic ratios were corrected for mass fractionation using the deviation of standards measured during the run over the natural ratio of the element (Table S2). External reproducibility on HSE analyses was better than 0.9% for 0.5 ppb solutions and all reported values are blank corrected. Total procedural blanks run with samples had $^{187}Os/^{188}Os = 0.22 \pm 0.09$ (n = 4; 1 s.d.), with quantities (in pg) of 0.5 ± 0.6 [Re], 11.9 ± 10.5 [Pd], 1.3 ± 0.7 [Pt], 10.2

192 ± 8.5 [Ru], 1.6 ± 1.3 [Ir] and 2.9 ± 1.1 [Os] (n=3; 1 s.d.) (see Table S3 for details). Repeat
193 measurements of BHVO-2 and OKUM-1 standards gave $^{187}Os/^{188}Os$ ratios of 0.15317 ± 0.02522
194 (n = 3) and 0.26471 ± 0.02373 (n = 3) respectively. HSE abundances are (in ng) 0.7 ± 0.02 [Re],
195 3.2 ± 0.3 [Pd], 14.2 ± 4.9 [Pt], 0.3 ± 0.02 [Ru], 0.1 ± 0.01 [Ir] and 0.3 ± 0.07 [Os] for BHVO-2
196 (n = 3; 1 s.d.) and 0.6 ± 0.002 [Re], 12.7 ± 0.8 [Pd], 11.1 ± 0.08 [Pt], 4.7 ± 0.02 [Ru], 1.0 ± 0.06
197 [Ir] and 1.2 ± 0.2 [Os] for OKUM-1 (n = 3; 1 s.d.). The HSE abundances and $^{187}Os/^{188}Os$ ratios
198 for OKUM-1 are consistent with those reported by Savard et al. (2010), Chen et al. (2016) and
199 Maier et al. (2012, 2017). Information regarding run statistics can be found in Tables S2 and S3.
200
201 Major and trace elements analyses were performed on 50 mg of homogenized whole rock
202 powder or powdered olivine, using a *Thermo Scientific* iCaP Qc ICP-MS using the method
203 outlined in Day et al. (2014). Samples were prepared and analyzed with powdered rock standards
204 (BHVO-2, BCR-2 and BIR-1a), to confirm accuracy, with reproducibility on most of trace
205 element abundances better than ± 5% (with the exception of Ba, Zr and Mo; see Tables S7 and
206 S8 for more information). We find that our new trace element data are in good agreement and
207 expand the available trace elements measured in previous studies (Baker et al., 1983; Farley et
208 al., 1993; Truong et al., 2018) using both XRF and ICP-MS methodologies. Trace element
209 abundances are reported in Table S6. Major element analyses were performed for the olivines to
210 complement the whole-rock dataset from Farley et al. (1993). We note that Juan Fernandez
211 olivine separates have high Al_2O_3 and TiO_2 content (0.4 – 1.2 wt% and 0.08 – 1.9 wt%
212 respectively) compared to other OIB olivine separates like those from Samoa (Jackson & Shirey,
213 2011; olivine Al_2O_3 content between 0.04 and 0.07 wt%, TiO_2 content between 0.01 and 0.03
214 wt%), likely reflecting impurities in the measured separates, including spinel grains. The

Robinson Crusoe rejuvenated olivine is enriched in incompatible elements compared to the main shield olivine from the same island (Figure 3). Moreover, the olivine grains in the three different samples display strong positive anomalies in titanium. This is explained by the abundance of chromian titanomagnetite inclusions in the olivine grains, as described by Natland (2003).

Characterization of the spinel inclusions in the olivine grains was performed using a Field Emission Gun Scanning Electron Microscopy (FEG-SEM) coupled with an EDS detector at the University of California San Diego. Map acquisition was performed using one frame count and a pixel dwell time of 100 µs. Spectra were acquired for 20 s. The major element compositions of the spinel inclusions in the olivine grains are reported in Table S4. In-situ HSE abundance analyses of spinel inclusions and olivine grains were performed at the SIGL using a *Thermo Scientific* iCaP Qc ICP-MS coupled with a *New Wave Research* UP213 Laser Ablation System. Ablation analysis took place in a 3 cm^3 ablation cell. The cell was flushed with a He-gas flow mixed with Ar as a carrier at ~ 1 $L.min^{-1}$. Signals were acquired in Time Resolved Acquisition, devoting around 15s for the blank and 30s for measurement of the analyses. Wash time between each analysis was 120 s. The laser was fired using an energy density of ~3.4 $J.cm^{-2}$ at a frequency of 5Hz. Standardization was performed using iron meteorites Hoba, Filomena and Coahuila as certified reference material, using preferred values reported by Day et al. (2018) for the HSE. Because the spinel inclusions were mostly smaller than the beam size, olivine grain compositions were also measured and proportionally subtracted from the spinel measurements. Even though HSE were detected in some of the olivine grains and their spinel inclusions, results were limited by the detection efficiency of the instrument and the sample size. The HSE abundances in the spinel inclusions and olivine grains are reported in Table S5.

238

239 **3. RESULTS**

240 **3.1. Characterization of inclusions in Juan Fernandez olivine grains**

241 Juan Fernandez olivine grains contain numerous inclusions that are mostly spinels (Figure 2
242 and Table S4), as previously described by Natland (2003). Spinel inclusions in Robinson Crusoe
243 and Alexander Selkirk main shield olivine grains have higher Cr# (55 ± 7; Cr/[Cr+Al] AFU) and
244 lower Mg# (43 ±4; Mg/[Mg+Fe] AFU; n = 16) than spinel grains in the rejuvenated lava (Cr# =
245 12 ± 6; Mg# = 66 ± 2; n = 4). Abundances of the HSE for olivine and spinel are reported in
246 Table S5. Spinel inclusions have generally elevated abundances of Re (~0.3 × CI chondrite), Ru,
247 Os and Pd (~0.12 × CI chondrite) and low Ir and Pt compared to their olivine host.

248

249 **3.2. Trace element abundances**

250 Trace element abundance measurements for Juan Fernandez Islands lavas and olivine
251 separates are reported in Table S6 and Figures 3 and S1. These new data expand upon - and are
252 in excellent agreement with - previously published Juan Fernandez datasets (Baker et al., 1983;
253 Farley et al., 1993; Truong et al., 2018). Juan Fernandez lavas show enrichment relative to
254 primitive mantle in high field strength elements (HFSE) Ti, Ta and Nb, as reported by Truong et
255 al. (2018), which are common features of most OIB (Jackson et al., 2008; Peters and Day, 2014).
256 The majority of Robinson Crusoe and Alexander Selkirk main shield lavas show positive
257 anomalies in Nb, Ta, Zr, and Sr, and slight negative anomalies in Y. Main shield lavas also have
258 similar rare earth element (REE) patterns with light REE (LREE) enrichments (Figure 3). In
259 contrast, Robinson Crusoe basanite lavas have higher absolute trace element abundances than
260 those from the main shield stage and higher Nb/Y at a given Zr/Y (Figures 3 and 4). This

261 characteristic is also observed in the olivine separates (Figure 3), which also display strong
262 positive anomalies in titanium (see *Supplementary Information*). Olivine separates have low Mo
263 and W abundances (<0.2 and <0.1 ppm, respectively) compared with main shield lavas from
264 Robinson Crusoe (Mo = 0.72 ± 0.09 ppm; W = 0.23 ± 0.09 ppm) and Alexander Selkirk (Mo =
265 0.84 ± 0.15 ppm; W = 0.44 ± 0.34 ppm), which in turn, have lower abundances of Mo and W
266 than the basanite lavas from Robinson Crusoe (Mo = 2.23 ± 0.18 ppm; W = 0.88 ± 0.13 ppm)
267 (Figure S2).
268
269 **3.3. Osmium isotope compositions and highly siderophile element abundances**
270 Rhenium-osmium isotope and HSE (Re, Pd, Pt, Ru, Ir, Os) abundance measurements for
271 Juan Fernandez Islands lavas and olivine separates are reported in Table 1. Ratios of $^{187}Os/^{188}Os$
272 were appropriately age-corrected to 4 Ma and 1 Ma, respectively, for the islands of Robinson
273 Crusoe and Alexander Selkirk and we refer to age-corrected values even though age-corrections
274 are negligible (Table 1). Low-Os lavas (10-50 ppt; PV-2, PF-16 Rpt, MF-16, MF-6 Rpt and MF-
275 C4) have variable to radiogenic isotopic compositions (0.1291 to 0.1435). For samples
276 (including olivine separates) with Os >50 ppt, $^{187}Os/^{188}Os$ ratios for Robinson Crusoe main
277 shield lavas are 0.1313 ± 0.0022 (Os = 65-910 ppt; 1 s.d., n = 7), with slightly less radiogenic
278 although overlapping values for Alexander Selkirk main shield lavas (0.1291 ± 0.0023; Os = 50-
279 276 ppt; 1 s.d., n = 5) (Figure 5). The least radiogenic lavas are the basanite samples from
280 Robinson Crusoe (0.1279 ± 0.0046; Os = 180-800 ppt; 1 s.d., n = 4). The osmium isotopic
281 compositions of Juan Fernandez lavas are generally less radiogenic than lavas from many other
282 OIB, and in the range of primitive mantle $^{187}Os/^{188}Os$ (0.1296 ± 0.0008; Meisel et al., 2001).
283

Olivine separates tend to be less radiogenic than their host lavas ([^{187}Os/^{188}Os Host - ^{187}Os/^{188}Os Olivine] × 1000 values range between 3.7 and 6.4), with ^{187}Os/^{188}Os ratios between 0.12709 and 0.13032 (0.1283 ± 0.0017), with Os concentrations between 21 and 138 ppt (Figure S3). The ^{187}Os/^{188}Os composition of the olivine separates are akin to those from Samoa (Jackson and Shirey, 2011) and from Iceland and Jan Mayen (Debaille et al., 2009), which also display high He isotope values.

Robinson Crusoe main shield lavas have relatively flat HSE patterns, approximately ten times lower than Primitive Mantle estimates (Day et al., 2017), with elevated Re contents (Figure 6a). Alexander Selkirk main shield lavas have generally lower absolute HSE abundances than Robinson Crusoe main shield lavas, with prominent Ru anomalies, and one sample also shows Pd and Ir enrichment (MF-16; Figure 6c). Sample MF-S1 also has anomalously high concentrations of Pt (>100 ppb); for clarity this datum is not shown in Figure 6. Robinson Crusoe basanites have a range of HSE abundances spanning those observed in the Robinson Crusoe and Alexander Selkirk main shield lavas (Figure 6b). Olivine separates tend to have lower HSE abundances compare to their host lava, with the exception of a strong positive Ru anomaly. Absolute HSE abundances of Juan Fernandez lavas are generally lower than for lavas from Hawaii (Ireland et al., 2009), Réunion (Peters et al., 2016) and the Canary Islands (Day et al., 2010), but show similar inter-element HSE variations (Figures 7 and S4).

4. DISCUSSION

4.1 Rejuvenated and main shield lavas and clarification of prior groupings

Flexural uplift of lithosphere in response to far-field stresses can lead to rejuvenated

307 volcanism. On mature oceanic plate, such as around Hawaii, uplift of the elastic lithosphere
308 occurs up to 200 km downstream from the active load, leading to decompression of the
309 underlying asthenosphere (e.g., Bianco et al., 2005) and generation of rejuvenated basaltic lavas
310 characterized by depleted isotopic signatures (e.g., Bizimis et al., 2013; Garcia et al., 2016) and
311 higher Nb/Y ratios at a given Zr/Y ratio than for main shield stage basalts (Figure 4), suggesting
312 distinct mantle sources for the main shield stage and rejuvenated stage lavas.
313
314 Post-erosional lavas from Robinson Crusoe bear many of the hallmarks of rejuvenated lavas
315 (see also, Reyes et al., 2017; Truong et al., 2018). These lavas are low-degree partial melts
316 (basanites; Figure S5) that are enriched in incompatible elements compared to the main shield
317 lavas from Robinson Crusoe, and also have relatively depleted Sr and Nd isotope signatures
318 (Baker et al., 1987; Farley et al., 1993; Reyes et al., 2017; Truong et al., 2018). As with Hawaii,
319 Robinson Crusoe rejuvenated lavas also have higher Nb/Y ratios at a given Zr/Y than those from
320 the main shield stage. We also find that these rejuvenated lavas span a larger range of HSE
321 abundances and have generally lower and more variable Os isotopes ratios than main shield lavas
322 (Figure 5). Because there is no correlation between HSE abundances with fractional
323 crystallization indicators like MgO (Figure S4), these variations likely reflect a greater degree of
324 lithospheric interaction, where the oceanic lithosphere has relatively unradiogenic Os isotopic
325 compositions and high HSE abundances (e.g., Day et al., 2017).
326
327 Generation of rejuvenated lavas on Robinson Crusoe at ~ 0.9 Ma ($^{40}Ar/^{39}Ar$ age reported for
328 one basanite from Santa Clara Island by Reyes et al., 2017) are consistent with loading of the
329 lithosphere by the formation of Alexander Selkirk (between 0.85 ± 0.3 Ma and 2.4 ± 0.1 Ma)

some 180 km away at a plate velocity of 6 km Ma^{-1}. Since the Robinson Crusoe basanites can be classified as rejuvenated lavas, we clarify that the previous compositional grouping scheme of Farley et al. (1993) for the basalts (Group I = Robinson Crusoe main shield; Group II = Robinson Crusoe basanites; Group III = Alexander Selkirk main shield) is consistent with the distinct volcanism mechanisms for their formation.

4.2 Crystal-liquid fractionation defines Juan Fernandez lava HSE compositions

During ascent through the oceanic crust towards the surface, mantle-derived magmas can assimilate significant volumes of crustal material, which can alter the HSE abundances and Os isotopic composition of the melt (e.g. Roy-Barman and Allègre, 1995; Lassiter and Hauri, 1998; Widom et al., 1999; Day et al., 2010). As Os is more compatible than Re during partial melting, large isotopic variations between mantle-derived materials ($^{187}Os/^{188}Os < 0.18$) and crustal or sedimentary materials occur with time ($^{187}Os/^{188}Os \geq 0.4$; Day, 2013). OIB with Os contents lower than 50 ppt are considered to be more susceptible to contamination by high $^{187}Os/^{188}Os$ crustal materials (e.g. Day, 2013). A few samples among Juan Fernandez lavas have low Os concentrations ($\leq$ 50 ppt), associated with radiogenic Os isotope compositions for two samples (MF-C4 = 0.13772 and PV-2 = 0.14349). Aside from these samples, assimilation processes play a limited role in Juan Fernandez main shield lava HSE compositions.

To quantify the role of fractional crystallization in the HSE fractionation for Juan Fernandez lavas, we used a model assuming olivine-melt and spinel-melt control using a calculated parental melt composition. The parent melt composition was obtained using a log-log variation diagram of Al_2O_3 versus MgO which allows discrimination between samples that

353 witnessed olivine and clinopyroxene accumulation or removal by a break in slope at ~11 to 12
354 wt.% Al_2O_3 and ~14 to 16 wt.% MgO. The parent melt composition was then derived from linear
355 regressions of HSE versus MgO trends at 15 ± 1 wt.%. These calculations indicate that the
356 parental melts of lavas from Robinson Crusoe and Alexander Selkirk have broadly similar HSE
357 contents. The amounts of early-formed spinel and olivine crystallization permissible for Juan
358 Fernandez lavas were calculated with Petrolog (Danyushevsky and Plechov, 2011) for fractional
359 crystallization of olivine and spinel at a range of pressures (1, 2, 5 and 10 kbar). Starting
360 compositions were chosen as closest to the parent melt composition (MgO = 15 wt.%) for each
361 of the three groups of lavas (PF-10, PF-16 and MF-C2 for Robinson Crusoe main shield lavas,
362 Robinson Crusoe rejuvenated lavas and Alexander Selkirk main shield lavas respectively). Major
363 element compositions for Juan Fernandez main shield lavas (e.g. Al_2O_3 or CaO contents in
364 function of MgO) can be explained by up to 30% of olivine fractionation (together with spinel
365 crystallization of up to 5%) between 1 to 5 kbar. On the other hand, Robinson Crusoe
366 rejuvenated lavas compositions can be reproduced at higher-pressure fractional crystallization
367 (up to 10 kbar): these mantle-derived melts experienced rapid ascent to the surface with a deeper
368 crystallization history. These results are consistent with Baker et al. (1987) and Reyes et al.
369 (2017) who suggested shallow storage conditions for the shield stage lavas (~ 1-3 kbar) and rapid
370 ascent with polybaric crystallization for the basanitic lavas (starting ~10 kbar).

371

372 Fractionation of olivine (up to 30%) alone from estimated parental melts produces
373 residual melts with HSE abundances similar to the observed compositions for Juan Fernandez
374 Islands but does not explain the shape of the observed HSE patterns, with a positive anomaly in
375 Ru (ol/melt partition coefficients from Puchtel and Humayun, 2001). Ruthenium, Ir and Os are

similarly compatible in olivine but Ru is highly compatible in spinel compared to the other HSE, and in particular to Ir and Os (e.g. Brenan et al., 2012). A notable feature of the Juan Fernandez olivine separates that we measured is a strong positive Ru anomaly (Figure 6). This can be explained by spinel crystallization and, then, inclusion in the olivine grains (Figure 2), further suggesting fractionation of both early-formed spinel and olivine. The method used to estimate the parent melt composition is associated with large uncertainties for HSE abundance estimates, which could explain why we are not able to reproduce the compositional range shown in Figure 8a. The incorporation of early-formed spinel (up to 5%) to the olivine grains can explain the generation of anomalously high Ru contents in olivine, due to the high compatibility of Ru in spinel (partition coefficients for sp/melt from Righter et al., (2004) for Re and Brenan et al. (2012) for Pd, Pt, Ir, Ru (see compilation in Day, 2013)).

Fractionation of up to 30% of olivine (ol/melt partition coefficients for REE from Fujimaki et al., 1984) from the most primitive lava from each of the three groups of the Juan Fernandez lavas produces REE patterns similar to those of the Juan Fernandez olivines for the HREE but that are too depleted for the LREE. The addition of 1 to 5% spinel (sp/melt partition coefficients for REE from Nagasawa et al., 1980) is also insufficient to reproduce the REE patterns we observe for Juan Fernandez olivine grains. However, the contamination by a small fraction (1 to 2% for the main shield lavas from both islands, up to 5% for the rejuvenated lavas) of the host lava (melt) is sufficient to enrich the olivine in LREE to the observed abundances, implying that silicate melt inclusions are also present in some olivine grains (Figure 9), which is consistent with petrographic observations (Natland, 2003). Contamination by the melt inclusions of the HSE signature of the olivine grains tends to lower the negative Pd anomaly of the

399 calculated composition, although overall, it has a limited effect on the HSE signature of the
400 olivine separates (Figure 8).
401
402 **4.3 Comparison of OIB main shield and rejuvenated lavas**
403
404 The Alexander Selkirk main shield lavas are lithologically and compositionally similar in
405 terms of major and trace element abundances to Robinson Crusoe main shield basalts (Baker et
406 al., 1987; Farley et al., 1993), whereas the Robinson Crusoe basanite lavas (rejuvenated lavas)
407 have higher abundances of incompatible trace elements, interpreted as resulting from lower
408 degrees of partial melting than for the main shield stage (Baker et al., 1987; Farley et al., 1993;
409 Reyes et al., 2017 and Figure S5). Samples from these three groups exhibit a large range in
410 $^{3}He/^{4}He$ ratios (7.8 to 18.0 R_A): Robinson Crusoe shield basalts have $^{3}He/^{4}He$ ratios between
411 13.6 and 18.0 R_A, whereas Robinson Crusoe post-shield basanites range from 11.2 to 12.9 R_A
412 (Farley et al., 1993; Truong et al., 2017). Main shield basalts from Alexander Selkirk show lower
413 and more uniform $^{3}He/^{4}He$ ratios with an average value of 8.3 ± 0.5 R_A (Farley et al., 1993).
414 Previous studies have shown limited variations for $^{87}Sr/^{86}Sr$ (0.70340–0.70378) and $^{143}Nd/^{144}Nd$
415 ratios (0.512835–0.512918) (Gerlach et al., 1986; Baker et al., 1987; Farley et al., 1993; Truong
416 et al., 2018). On average, Robison Crusoe main shield basalts are the most isotopically
417 heterogeneous in terms of Sr and Nd isotopic composition, while the rejuvenated basanites lie at
418 the most depleted end of the trend defined by Robinson Crusoe main shield basalts (lower
419 $^{87}Sr/^{86}Sr$ and higher $^{143}Nd/^{144}Nd$). Main shield basalts from Alexander Selkirk show
420 homogeneous compositions, with higher $^{143}Nd/^{144}Nd$ at a given $^{87}Sr/^{86}Sr$ than those from
421 Robinson Crusoe. Robinson Crusoe basalts and basanites have slightly more radiogenic

422 $^{206}Pb/^{204}Pb$ ratios (19.163 to 19.292) than Alexander Selkirk basalts (18.939 to 19.221) (Truong
423 et al., 2018). Overall, Sr-Nd-Pb isotopic compositions suggest that all the samples are from a
424 common, albeit slightly heterogeneous mantle source (Gerlach et al., 1986; Baker et al., 1987;
425 Farley et al., 1993; Truong et al., 2018).
426
427 Alexander Selkirk main shield lavas have been dated between 0.83-0.94 Ma (Lara et al.,
428 2018b), ca. 2 to 3 Ma younger than Robinson Crusoe main shield lavas. A $^{40}Ar/^{39}Ar$ age of 0.9 ±
429 0.03 Ma has also been reported by Reyes et al. (2017) for a basanite from Santa Clara Island.
430 Even though no radiometric ages are available for Robinson Crusoe rejuvenated lavas, they are
431 clearly younger as they intruded or cross-cut the main shield lavas (Reyes et al., 2017). They are
432 most likely to be contemporaneous with the creation of Alexander Selkirk Island. Robinson
433 Crusoe rejuvenated basanites have slightly less radiogenic and more variable $^{187}Os/^{188}Os$ ratios
434 than Alexander Selkirk main shield lavas, associated with higher $^{3}He/^{4}He$ values (11.2 to 12.9
435 R_A for Robinson Crusoe rejuvenated lavas, and 7.8 to 9.5 R_A for Alexander Selkirk main shield
436 lavas).
437
438 Konter and Jackson (2012) reported $^{187}Os/^{188}Os$ ratios for Samoan rejuvenated lavas that are
439 similar to $^{187}Os/^{188}Os$ ratios for Samoan peridotite xenoliths (Jackson et al., 2016), and exhibit
440 lower those for the Samoan main shield lavas (Figure 10). The Samoan xenoliths most likely
441 originate from within the mantle lithosphere (Hauri and Hart, 1994), such that the Os isotope
442 values in Samoan rejuvenated lavas are derived from the lithospheric mantle, suggesting melting
443 during Samoan rejuvenation stage occurs close to the lithosphere-asthenosphere boundary
444 (Konter and Jackson, 2012). Additionally, Samoan rejuvenated lavas have lower in $^{206}Pb/^{204}Pb$

445 and $^{208}Pb/^{204}Pb$, and intermediate in $^{87}Sr/^{86}Sr$ and $^{143}Nd/^{144}Nd$ compared to the shield lavas
446 (Figure S6 and Konter and Jackson, 2012). These later observations are also consistent with
447 sampling of a lithospheric component (Konter and Jackson, 2012). Hawaiian rejuvenated lavas,
448 on the other hand, have highly variable Os isotope compositions than range to more radiogenic
449 values than the main shield lavas, similar to pyroxenite xenoliths (Figure 10), whereas peridotite
450 xenoliths have subchondritic Os ratios (Lassiter et al., 2000; Bizimis et al., 2007; Sen et al.,
451 2011). Hawaiian rejuvenated lavas also have more depleted Sr- (and Nd-) isotope compositions
452 than the main shield lavas (Figure S6). Lassiter et al. (2000) proposed that moderate-degree
453 pyroxenite partial melts in the source of the rejuvenated lavas are most likely the source of the
454 radiogenic Os isotope signature due to correlations between Os isotopes and both major and trace
455 element abundances in the rejuvenated lavas. These results indicate strong similarities in
456 rejuvenated lavas from Juan Fernandez, Samoa and Hawaii.
457
458 The Robinson Crusoe basanites also exhibit depleted Sr and Nd isotopes signatures (Baker et
459 al., 1987; Farley et al., 1993; Reyes et al. 2017; Truong et al., 2018) compared to Robinson
460 Crusoe main shield lavas, and have lower $^{143}Nd/^{144}Nd$ at a given $^{87}Sr/^{86}Sr$ than Alexander Selkirk
461 main shield lavas. No distinction is observed between the three types of lavas in terms of
462 $^{207}Pb/^{204}Pb$. However, Alexander Selkirk main shield lavas are less radiogenic in Pb isotopes
463 than Robinson Crusoe main shield and rejuvenated lavas, which have overlapping $^{206}Pb/^{204}Pb$
464 and $^{208}Pb/^{204}Pb$. Thus, the relative sense of isotopic variability in Juan Fernandez main shield and
465 rejuvenated lavas is similar to those in Samoan and Hawaiian main shield and rejuvenated lavas
466 (Garcia et al., 2010; Konter and Jackson, 2012), and are consistent with a lithospheric source for
467 rejuvenated lavas (Bianco et al., 2005; Konter and Jackson 2012).

As noted above, Robinson Crusoe rejuvenated lavas have higher $^{3}He/^{4}He$ values than Alexander Selkirk main shield lavas and lower than Robinson Crusoe main shield lavas. We propose that the lithosphere was polluted by noble gases from the main shield building phase of Robinson Crusoe Island, during the ascent of the melts through the lithosphere, which then contaminated Robinson Crusoe rejuvenated melts explaining their elevated $^{3}He/^{4}He$ signatures. Model mixtures of a MORB-like depleted component (D) and a high-^{3}He hotspot endmember (P) are presented in Figure 11 and show that Robinson Crusoe rejuvenated lavas lie between the main shield lavas from Robinson Crusoe and Alexander Selkirk (curves B and C), and correspond to 40 to 60% of contamination of the depleted mantle component by a degassed plume component (curves B and C), corresponding to an open-system where the plume component would have been degassed of its mantle-derived He. This is similar to the mixing model proposed by Farley et al. (1993) between two endmembers Primitive Helium Mantle (PHEM) and the depleted MORB mantle (DMM) to reproduce Juan Fernandez lavas compositions.

4.4 Implications for high-$^{3}He/^{4}He$ and heterogeneous mantle plumes

Amongst OIB, Juan Fernandez lavas span an unusual isotopic compositional range: Juan Fernandez lavas overlap with Samoan lavas that are close to FOZO or C in terms of $^{187}Os/^{188}Os$, $^{206}Pb/^{204}Pb$, $^{208}Pb/^{204}Pb$ and $^{143}Nd/^{144}Nd$ ratios, but have lower $^{3}He/^{4}He$ ratios, intermediate between high-$^{3}He/^{4}He$ OIB (like Samoan, Icelandic and Hawaiian lavas) and low-$^{3}He/^{4}He$ OIB (Canary Islands and the Comores) (Figure 12). Overall, Juan Fernandez lavas converge at FOZO or C of the global OIB dataset e.g. Hart et al., 1992; Hanan and Graham, 1996; Day et al., 2010;

Truong et al., 2018). Juan Fernandez Islands display isotopic characteristics of a considerable range in $^{3}He/^{4}He$ (7.8 to 18 R_A), but limited variability in Sr, Nd, Pb and Os isotopic ratios. Whereas HSE and trace element abundances are controlled by melting and fractional crystallization, isotopic compositions of the Juan Fernandez lavas seem unaffected by fractional crystallization and assimilation processes. In particular, fractional crystallization and other petrogenetic processes cannot account for the high $^{3}He/^{4}He$ in Juan Fernandez lavas, as no correlation is observed between $^{3}He/^{4}He$ ratios and fractionation indicators like MgO. Thus, it seems that $^{3}He/^{4}He$ and bulk He of Juan Fernandez lavas are derived from the mantle plume and the differentiation processes experienced by the parent melts derived from this source, and not from volatiles that permeated shallow magma reservoirs (Natland, 2003).

Mantle plume sources can vary significantly in $^{3}He/^{4}He$ temporally and spatially, such as Samoa (19.5 to 33.8 R_A - Jackson et al., 2007), Hawaii (6 to 28 R_A - Mukhopadhyay et al., 2003; up to 29.3 R_A - Valbracht et al., 1997)) and Iceland (9.6 to 19 R_A - Brandon et al., 2007; up to 37.7 R_A - Hilton et al., 1999; and even 47.5 R_A - Harðardóttir et al., 2018). Variations in $^{3}He/^{4}He$ ratios are also observed for Juan Fernandez Islands: starting with inception of high $^{3}He/^{4}He$ (Robinson Crusoe main shield lavas) that also impregnates the lithosphere with ^{3}He (Robinson Crusoe rejuvenated lavas) followed by lower $^{3}He/^{4}He$ in Alexander Selkirk. Robinson Crusoe and Alexander Selkirk main shield lavas, however, are distinct in terms of radiogenic (Sr-Nd-Pb-Os) and noble gas (He) isotope compositions. Within the Juan Fernandez Islands, Robinson Crusoe main shield lavas are the most enriched samples with lower $^{143}Nd/^{144}Nd$ and higher $^{206}Pb/^{204}Pb$, $^{208}Pb/^{204}Pb$, $^{187}Os/^{188}Os$ and $^{3}He/^{4}He$ compared to Alexander Selkirk main shield

513 lavas. The distinction between Robinson Crusoe and Alexander Selkirk main shield lavas
514 suggests an isotopic zonation in the mantle plume.
515
516 Huang et al. (2011) showed that geochemical zoning might be a common feature of mantle
517 plumes beneath the Pacific plate: two subparallel arrays of volcanoes exist at Hawaii, Samoa,
518 and the Marquesas, with the southern trend of volcanoes being more radiogenic in lead and less
519 radiogenic in neodymium. Huang et al. (2011) proposed that isotopically enriched material is
520 preferentially distributed in the lower mantle of the Southern Hemisphere, within the Pacific low
521 seismic velocity zone. The distribution of heterogeneity in the Thermal Boundary Layer would
522 result in bilaterally zoned plume conduits at Hawaii and the Marquesas, Samoa being more
523 complex. A bilaterally zoned plume model has previously been proposed for the Hawaiian plume
524 (Abouchami et al., 2005). Weis et al. (2011) proposed that the geochemical differences between
525 the Kea and Loa trends reflect preferential sampling of two distinct sources of deep mantle
526 material: the Loa trend sampling LLSVP (Large Low-Shear Velocity Province) material, and the
527 Kea trend sampling lower mantle material. Alternatively, Farnetani & Hofmann (2009, 2010)
528 have proposed that a continuous deep layer overlained by a bilaterally varying layer best
529 reproduce the "bilateral asymmetry" observed for Pb isotopic differences between the Kea and
530 Loa-trends of Hawaiian volcanoes and for the concentric distribution of $^{3}He/^{4}He$ (DePaolo et al.,
531 2001). It has also been suggested that high-$^{3}He/^{4}He$ materials could be distributed as isolated
532 primitive blobs in the lower mantle (Becker et al., 1999), or in an isolated primitive reservoir in
533 the lower mantle (Allègre et al., 1983; Tolstikhin and Hofmann, 2005) or even in the core
534 (Bouhifd et al., 2013), to explain the isotopic variability observed within individual hotspot
535 tracks.

536

537 The Juan Fernandez Islands do not show a double volcanic chain, unlike Hawaii and the
538 other volcanic chains investigated by Huang et al. (2011). Sampling resolution on Juan
539 Fernandez lavas does not allow us to identify two geochemical trends in the isotopic data
540 between Robinson Crusoe and Alexander Selkirk. However, the isotopic variability in the mantle
541 plume observed between the main shield lavas of the two islands could be due to a variety of
542 models including a compositionally heterogeneous mantle source, with heterogeneities being
543 vertically stretched and rising at different rates inside the plume conduit (e.g., Farnetani &
544 Hofmann, 2010), sampling of lower mantle (e.g. Allègre et al., 1983; Tolstikhin and Hofmann,
545 2005) and LLSVP material (e.g., Weis et al., 2011).

546

547 The origin of the isotopically depleted component in hotspots is debated: it has been
548 proposed as (1) entrained upper mantle (e.g. Lassiter et al., 2000; Regelous et al., 2003), (2)
549 metasomatized lithospheric mantle (e.g. Pilet et al., 2008; Sorbadere et al., 2013), (3) intrinsic to
550 the plume (e.g. Yang et al., 2003; Mukhopadhyay et al., 2003; Frey et al., 2005; DeFelice et al.,
551 2019) or (4) subducted ancient lithospheric mantle (Castillo, 2015; Truong et al., 2018). The
552 Samoan depleted component is thought to be entrained depleted mantle (e.g. Konter and Jackson,
553 2012), whereas all the first three sources have been proposed for the depleted component in the
554 Galapagos (e.g. Blichert-Toft and White, 2001; Saal et al., 2007) and Icelandic plumes (e.g.
555 Fitton et al., 1997; Hanan et al., 2000; Chauvel et al., 2000). For the Hawaiian lavas, the depleted
556 component has been proposed to be an isotopically depleted component intrinsic to the plume
557 (e.g., Yang et al., 2003; Mukhopadhyay et al., 2003; Frey et al., 2005; DeFelice et al., 2019), the
558 lithospheric mantle (e.g. Lassiter et al., 2000) or even the Pacific DMM (e.g. Keller et al., 2000).

559 The addition of a depleted MORB-like mantle component well explains the isotopic composition
560 of Alexander Selkirk main shield lavas, with the isotopic signature of these lavas being
561 consistent with sampling of FOZO and a more depleted component (Figure 11). However a
562 higher contribution of this depleted component to the compositions of Alexander Selkirk lavas
563 should produce depleted trace element patterns relative to Robinson Crusoe main shield lavas,
564 which is not what we observed (Figure 3). Thus, even if Alexander Selkirk main shield lavas are
565 slightly more isotopically depleted relative to those from Robinson Crusoe, they might still
566 sample a heterogeneous FOZO domain, possibly distinct from the DMM, to produce such trace
567 element compositions.
568
569 **5. CONCLUSIONS**
570 We present new major-, trace- and highly siderophile- element abundances (HSE: Re, Pd, Pt,
571 Ru, Ir, Os) and Os isotope compositions for a suite of lavas and olivine separates from the Juan
572 Fernandez Islands. We clarify the previous grouping scheme of Farley et al. (1993) for the
573 basalts after showing that Robinson Crusoe basanites are rejuvenated lavas. The fractionation of
574 an assemblage of 30 modal % olivine and 1-5 modal % spinel, plus a small contribution of the
575 primary melt from olivine melt inclusions (1 to 2% for both main shield lavas, up to 5% for the
576 rejuvenated lavas), recreates HSE patterns for olivine grains in samples and also reproduces the
577 range of HSE compositions observed in Juan Fernandez lavas, consistent with modeling of REE
578 abundances in the olivine separates. Overall, Juan Fernandez lavas sample the convergence zone
579 of all OIB, at the "FOZO" or "C" component. Robinson Crusoe basanite lavas represent
580 rejuvenated volcanism dominantly from a depleted lithospheric mantle source ($^{187}Os/^{188}Os$
581 <0.13) polluted by high-$^{3}He/^{4}He$ from the main shield building stage of the island. Robinson

582 Crusoe main shield lavas sample a high-$^{3}He/^{4}He$ (>18R_A) and enriched mantle source
583 ($^{187}Os/^{188}Os$ = 0.1312) akin to the FOZO or C component, whereas Alexander Selkrik lavas are
584 from a dominant contribution from a depleted mantle component with low-$^{3}He/^{4}He$ (<10R_A).
585 Apart from their He signature, these mantle sources of the shield lavas show limited variations
586 for the other radiogenic isotopes, and no clear variations of the HSE or trace elements, likely due
587 to limited differences in the source composition and degree of partial melting. We propose that
588 Robinson Crusoe form during an initial eruption stage of lavas from a primitive high-$^{3}He/^{4}He$
589 mantle source ~4 Ma, which also led to noble gas impregnation of the oceanic lithosphere. This
590 first stage was followed by eruption of Alexander Selkirk lavas from a more depleted mantle
591 source at ~ 2 Ma. Mantle heterogeneity preserved in Juan Fernandez lavas over short timescales
592 (<2 Ma) and can impact lithospheric compositions, resulting in formation of rejuvenated lavas
593 with unique isotopic compositions.
594

595 **ACKNOWLEDGEMENTS**

596 We thank Jasper Konter, two anonymous reviewers, and the Associate Editor, Shichun Huang,
597 for their helpful comments. This work was supported by the National Science Foundation (EAR-
598 1116089; EAR-1447130). We are grateful to Emily Chin and Sarah Perry for analytical
599 assistance with the secondary electron microscope.
600

601 **REFERENCES**

602 Abouchami, W., Hofmann, A. W., Galer, S. J. G., Frey, F. A., Eisele, J., & Feigenson, M. (2005).
603 Lead isotopes reveal bilateral asymmetry and vertical continuity in the Hawaiian mantle
604 plume. *Nature*, *434*(7035), 851.

605 Allègre, C. J., Staudacher, T., Sarda, P., & Kurz, M. (1983). Constraints on evolution of Earth's
606 mantle from rare gas systematics. *Nature*, *303*(5920), 762.

607 Baker, P. E., Gledhill, A., Harvey, P. K., & Hawkesworth, C. J. (1987). Geochemical evolution of
608 the Juan Fernandez islands, SE Pacific. *Journal of the Geological Society*, *144*(6), 933-944.

609 Becker, T. W., Kellogg, J. B., & O'Connell, R. J. (1999). Thermal constraints on the survival of
610 primitive blobs in the lower mantle. *Earth and Planetary Science Letters*, *171*(3), 351-365.

611 Bennett, V. C., Norman, M. D., & Garcia, M. O. (2000). Rhenium and platinum group element
612 abundances correlated with mantle source components in Hawaiian picrites: sulphides in the
613 plume. *Earth and Planetary Science Letters*, *183*(3), 513-526.

614 Bianco, T. A., Ito, G., Becker, J. M., & Garcia, M. O. (2005). Secondary Hawaiian volcanism
615 formed by flexural arch decompression. *Geochemistry, Geophysics, Geosystems*, *6*(8).

616 Birck, J. L., Barman, M. R., & Capmas, F. (1997). Re-Os isotopic measurements at the femtomole
617 level in natural samples. *Geostandards and Geoanalytical Research*, *21*(1), 19-27.

618 Bizimis, M., Griselin, M., Lassiter, J. C., Salters, V. J., & Sen, G. (2007). Ancient recycled mantle
619 lithosphere in the Hawaiian plume: osmium–hafnium isotopic evidence from peridotite
620 mantle xenoliths. *Earth and Planetary Science Letters*, *257*(1-2), 259-273.

621 Bizimis, M., Salters, V. J., Garcia, M. O., & Norman, M. D. (2013). The composition and
622 distribution of the rejuvenated component across the Hawaiian plume: Hf-Nd-Sr-Pb isotope

623 systematics of Kaula lavas and pyroxenite xenoliths. *Geochemistry, Geophysics,*
624 *Geosystems*, *14*(10), 4458-4478.
625 Blichert-Toft, J., & White, W. M. (2001). Hf isotope geochemistry of the Galapagos
626 Islands. *Geochemistry, Geophysics, Geosystems*, *2*(9).
627 Booker, J., Bullard, E. C., & Grasty, R. L. (1967). Palaeomagnetism and age of rocks from Easter
628 Island and Juan Fernandez. *Geophysical Journal International*, *12*(5), 469-471.
629 Bouhifd, M. A., Jephcoat, A. P., Heber, V. S., & Kelley, S. P. (2013). Helium in Earth's early
630 core. *Nature Geoscience*, *6*(11), 982.
631 Brandon, A. D., & Walker, R. J. (2005). The debate over core–mantle interaction. *Earth and*
632 *Planetary Science Letters*, *232*(3-4), 211-225.
633 Brandon, A. D., Graham, D. W., Waight, T., & Gautason, B. (2007). ^{186}Os and ^{187}Os enrichments
634 and high-$^{3}He/^{4}He$ sources in the Earth's mantle: evidence from Icelandic
635 picrites. *Geochimica et Cosmochimica Acta*, *71*(18), 4570-4591.
636 Brenan, J. M., Finnigan, C. F., McDonough, W. F., & Homolova, V. (2012). Experimental
637 constraints on the partitioning of Ru, Rh, Ir, Pt and Pd between chromite and silicate melt:
638 the importance of ferric iron. *Chemical Geology*, *302*, 16-32.
639 Bryce, J. G., DePaolo, D. J., & Lassiter, J. C. (2005). Geochemical structure of the Hawaiian
640 plume: Sr, Nd, and Os isotopes in the 2.8 km HSDP‐2 section of Mauna Kea
641 volcano. *Geochemistry, Geophysics, Geosystems*, *6*(9).
642 Castillo, P.R. (2015) The recycling of marine carbonates and sources of HIMU and FOZO ocean
643 island basalts. *Lithos,* 216, 254–263.

644 Chauvel, C., & Hémond, C. (2000). Melting of a complete section of recycled oceanic crust: Trace
645 element and Pb isotopic evidence from Iceland. *Geochemistry, Geophysics,*
646 *Geosystems*, *1*(2).
647 Chen, K., Walker, R. J., Rudnick, R. L., Gao, S., Gaschnig, R. M., Puchtel, I. S., ... & Hu, Z. C.
648 (2016). Platinum-group element abundances and Re–Os isotopic systematics of the upper
649 continental crust through time: Evidence from glacial diamictites. *Geochimica et*
650 *Cosmochimica Acta*, *191*, 1-16.
651 Class, C., Goldstein, S. L., Altherr, R., & Bachèlery, P. (1998). The process of plume–lithosphere
652 interactions in the ocean basins—the case of Grande Comore. *Journal of Petrology*, *39*(5),
653 881-903.
654 Class, C., Goldstein, S. L., Stute, M., Kurz, M. D., & Schlosser, P. (2005). Grand Comore Island:
655 a well-constrained "low $^{3}He/^{4}He$" mantle plume. *Earth and Planetary Science*
656 *Letters*, *233*(3), 391-409.
657 Class, C., Goldstein, S. L., & Shirey, S. B. (2009). Osmium isotopes in Grande Comore lavas: a
658 new extreme among a spectrum of EM-type mantle endmembers. *Earth and Planetary*
659 *Science Letters*, *284*(1), 219-227.
660 Cohen, A. S., & Waters, F. G. (1996). Separation of osmium from geological materials by solvent
661 extraction for analysis by thermal ionisation mass spectrometry. *Analytica Chimica*
662 *Acta*, *332*(2), 269-275.
663 Danyushevsky, L. V., & Plechov, P. (2011). Petrolog3: Integrated software for modeling
664 crystallization processes. *Geochemistry, Geophysics, Geosystems*, *12*(7).
665 Day J. M. D. (2013) Hotspot volcanism and highly siderophile elements. *Chemical Geology*, 341,
666 50-74.

667 Day, J. M. D., & Hilton, D. R. (2011). Origin of $^{3}He/^{4}He$ ratios in HIMU-type basalts constrained
668 from Canary Island lavas. *Earth and Planetary Science Letters*, *305*(1), 226-234.
669 Day, J. M. D., Pearson, D. G., Macpherson, C. G., Lowry, D., & Carracedo, J. C. (2010). Evidence
670 for distinct proportions of subducted oceanic crust and lithosphere in HIMU-type mantle
671 beneath El Hierro and La Palma, Canary Islands. *Geochimica et Cosmochimica*
672 *Acta*, *74*(22), 6565-6589.
673 Day, J. M. D., Peters, B. J., & Janney, P. E. (2014). Oxygen isotope systematics of South African
674 olivine melilitites and implications for HIMU mantle reservoirs. *Lithos*, *202*, 76-84.
675 Day, J. M. D., Waters, C. L., Schaefer, B. F., Walker, R. J., & Turner, S. (2016). Use of
676 Hydrofluoric Acid Desilicification in the Determination of Highly Siderophile Element
677 Abundances and Re-Pt-Os Isotope Systematics in Mafic-Ultramafic Rocks. *Geostandards*
678 *and Geoanalytical Research*, *40*(1), 49-65.
679 Day, J. M. D., Walker, R. J., & Warren, J. M. (2017). $^{186}Os–^{187}Os$ and highly siderophile element
680 abundance systematics of the mantle revealed by abyssal peridotites and Os-rich
681 alloys. *Geochimica et Cosmochimica Acta*, *200*, 232-254.
682 Day, J. M. D., Maria-Benavides, J., McCubbin, F. M., & Zeigler, R. A. (2018). The potential for
683 metal contamination during Apollo lunar sample curation. *Meteoritics & Planetary*
684 *Science*, *53*(6), 1283-1291.
685 Debaille, V., Trønnes, R. G., Brandon, A. D., Waight, T. E., Graham, D. W., & Lee, C. T. A.
686 (2009). Primitive off-rift basalts from Iceland and Jan Mayen: Os-isotopic evidence for a
687 mantle source containing enriched subcontinental lithosphere. *Geochimica et Cosmochimica*
688 *Acta*, *73*(11), 3423-3449.

689 DeFelice, C., Mallick, S., Saal, A. E., & Huang, S. (2019). An isotopically depleted lower mantle
690 component is intrinsic to the Hawaiian mantle plume. *Nature Geoscience*, *12*(6), 487.
691 DeMets, C., Gordon, R. G., & Argus, D. F. (2010). Geologically current plate
692 motions. *Geophysical Journal International*, *181*(1), 1-80.
693 DePaolo, D. J., Bryce, J. G., Dodson, A., Shuster, D. L., & Kennedy, B. M. (2001). Isotopic
694 evolution of Mauna Loa and the chemical structure of the Hawaiian plume. *Geochemistry,*
695 *Geophysics, Geosystems*, *2*(7).
696 Devey, C. W., Hémond, C., & Stoffers, P. (2000). Metasomatic reactions between carbonated
697 plume melts and mantle harzburgite: the evidence from Friday and Domingo Seamounts
698 (Juan Fernandez chain, SE Pacific). *Contributions to Mineralogy and Petrology*, *139*(1), 68-
699 84.
700 Farley, K. A., Natland, J. H., & Craig, H. (1992). Binary mixing of enriched and undegassed
701 (primitive?) mantle components (He, Sr, Nd, Pb) in Samoan lavas. *Earth and Planetary*
702 *Science Letters*, *111*(1), 183-199.
703 Farley, K. A., Basu, A. R., & Craig, H. (1993). He, Sr and Nd isotopic variations in lavas from the
704 Juan Fernandez Archipelago, SE Pacific. *Contributions to Mineralogy and*
705 *Petrology*, *115*(1), 75-87.
706 Farnetani, C. G., & Hofmann, A. W. (2009). Dynamics and internal structure of a lower mantle
707 plume conduit. *Earth and Planetary Science Letters*, *282*(1-4), 314-322.
708 Farnetani, C. G., & Hofmann, A. W. (2010). Dynamics and internal structure of the Hawaiian
709 plume. *Earth and Planetary Science Letters*, *295*(1-2), 231-240.

710 Fitton, J. G., Saunders, A. D., Norry, M. J., Hardarson, B. S., & Taylor, R. N. (1997). Thermal and
711 chemical structure of the Iceland plume. *Earth and Planetary Science Letters*, *153*(3-4),
712 197-208.
713 Frey, F. A., Huang, S., Blichert-Toft, J., Regelous, M., & Boyet, M. (2005). Origin of depleted
714 components in basalt related to the Hawaiian hot spot: Evidence from isotopic and
715 incompatible element ratios. *Geochemistry, Geophysics, Geosystems*, *6*(2).
716 Frey, F. A., Huang, S., Xu, G., & Jochum, K. P. (2016). The geochemical components that
717 distinguish Loa-and Kea-trend Hawaiian shield lavas. *Geochimica et Cosmochimica*
718 *Acta*, *185*, 160-181.
719 Fujimaki, H., Tatsumoto, M., & Aoki, K. I. (1984). Partition coefficients of Hf, Zr, and REE
720 between phenocrysts and groundmasses. *Journal of Geophysical Research: Solid*
721 *Earth*, *89*(S02), B662-B672.
722 Garcia, M. O., Rhodes, J. M., Wolfe, E. W., Ulrich, G. E., & Ho, R. A. (1992). Petrology of lavas
723 from episodes 2–47 of the Puu O'o eruption of Kilauea Volcano, Hawaii: evaluation of
724 magmatic processes. *Bulletin of Volcanology*, *55*(1-2), 1-16.
725 Garcia, M. O., Rhodes, J. M., Trusdell, F. A., & Pietruszka, A. J. (1996). Petrology of lavas from
726 the Puu Oo eruption of Kilauea Volcano: III. The Kupaianaha episode (1986–1992). *Bulletin*
727 *of Volcanology*, *58*(5), 359-379.
728 Garcia, M. O., Pietruszka, A. J., Rhodes, J. M., & Swanson, K. (2000). Magmatic processes
729 during the prolonged Pu'u'O'o eruption of Kilauea Volcano, Hawaii. *Journal of*
730 *Petrology*, *41*(7), 967-990.
731 Garcia, M. O., Swinnard, L., Weis, D., Greene, A. R., Tagami, T., Sano, H., & Gandy, C. E.
732 (2010). Petrology, geochemistry and geochronology of Kaua 'i lavas over 4·5 Myr:

733 Implications for the origin of rejuvenated volcanism and the evolution of the Hawaiian
734 plume. *Journal of Petrology*, *51*(7), 1507-1540.
735 Garcia, M. O., Weis, D., Jicha, B. R., Ito, G., & Hanano, D. (2016). Petrology and geochronology
736 of lavas from Ka ʻula Volcano: Implications for rejuvenated volcanism of the Hawaiian
737 mantle plume. *Geochimica et Cosmochimica Acta*, *185*, 278-301.
738 Gerlach, D. C., Hart, S. R., Morales, V. W. J., & Palacios, C. (1986). Mantle heterogeneity
739 beneath the Nazca plate: San Felix and Juan Fernandez islands. *Nature*, *322*(6075), 165-169.
740 Graham, D. W. (2002). Noble gas isotope geochemistry of mid-ocean ridge and ocean island
741 basalts: Characterization of mantle source reservoirs. *Reviews in mineralogy and*
742 *geochemistry*, *47*(1), 247-317.
743 Hanan, B. B., Blichert-Toft, J., Kingsley, R., & Schilling, J. G. (2000). Depleted Iceland mantle
744 plume geochemical signature: Artifact of multicomponent mixing?. *Geochemistry,*
745 *Geophysics, Geosystems*, *1*(4).
746 Hanan, B. B., & Graham, D. W. (1996). Lead and helium isotope evidence from oceanic basalts
747 for a common deep source of mantle plumes. *Science*, *272*(5264), 991-995.
748 Harðardóttir, S., Halldórsson, S. A., & Hilton, D. R. (2018). Spatial distribution of helium isotopes
749 in Icelandic geothermal fluids and volcanic materials with implications for location,
750 upwelling and evolution of the Icelandic mantle plume. *Chemical Geology*, *480*, 12-27.
751 Hart, S. R., Hauri, E. H., Oschmann, L. A., & Whitehead, J. A. (1992). Mantle plumes and
752 entrainment: isotopic evidence. *Science*, *256*(5056), 517-520.
753 Haskins, E. H., & Garcia, M. O. (2004). Scientific drilling reveals geochemical heterogeneity
754 within the Ko'olau shield, Hawaii. *Contributions to Mineralogy and Petrology*, *147*(2), 162-
755 188.

Hauri, E. H., & Hart, S. R. (1993). Re-Os isotope systematics of HIMU and EMII oceanic island basalts from the south Pacific Ocean. *Earth and Planetary Science Letters*, *114*(2-3), 353-371.

Hauri, E. H., & Hart, S. R. (1994). Constraints on melt migration from mantle plumes: a trace element study of peridotite xenoliths from Savai'i, Western Samoa. *Journal of Geophysical Research: Solid Earth*, *99*(B12), 24301-24321.

Hilton, D. R., Macpherson, C. G., & Elliott, T. R. (2000). Helium isotope ratios in mafic phenocrysts and geothermal fluids from La Palma, the Canary Islands (Spain): implications for HIMU mantle sources. *Geochimica et Cosmochimica Acta*, *64*(12), 2119-2132.

Hilton, D. R., Grönvold, K., Macpherson, C. G., & Castillo, P. R. (1999). Extreme $^{3}He/^{4}He$ ratios in northwest Iceland: constraining the common component in mantle plumes. *Earth and Planetary Science Letters*, *173*(1-2), 53-60.

Hoernle, K., Werner, R., Morgan, J. P., Garbe-Schönberg, D., Bryce, J., & Mrazek, J. (2000). Existence of complex spatial zonation in the Galápagos plume. *Geology*, *28*(5), 435-438.

Hofmann, A. W. (2014). Sampling mantle heterogeneity through oceanic basalts: isotopes and trace elements. *Treatise on geochemistry*, *3*, 67-101.

Huang, S., Hall, P. S., & Jackson, M. G. (2011). Geochemical zoning of volcanic chains associated with Pacific hotspots. *Nature Geoscience*, *4*(12), 874.

Ireland, T. J., Walker, R. J., & Garcia, M. O. (2009). Highly siderophile element and ^{187}Os isotope systematics of Hawaiian picrites: implications for parental melt composition and source heterogeneity. *Chemical Geology*, *260*(1), 112-128.

777 Jackson, M. G., & Shirey, S. B. (2011). Re–Os isotope systematics in Samoan shield lavas and the
778 use of Os-isotopes in olivine phenocrysts to determine primary magmatic
779 compositions. *Earth and Planetary Science Letters*, *312*(1), 91-101.
780 Jackson, M. G., Kurz, M. D., Hart, S. R., & Workman, R. K. (2007). New Samoan lavas from Ofu
781 Island reveal a hemispherically heterogeneous high $^{3}He/^{4}He$ mantle. *Earth and Planetary*
782 *Science Letters*, *264*(3), 360-374.
783 Jackson, M. G., Hart, S. R., Saal, A. E., Shimizu, N., Kurz, M. D., Blusztajn, J. S., & Skovgaard,
784 A. C. (2008). Globally elevated titanium, tantalum, and niobium (TITAN) in ocean island
785 basalts with high $^{3}He/^{4}He$. *Geochemistry, Geophysics, Geosystems*, *9*(4).
786 Jackson, M. G., Hart, S. R., Konter, J. G., Kurz, M. D., Blusztajn, J., & Farley, K. A. (2014).
787 Helium and lead isotopes reveal the geochemical geometry of the Samoan
788 plume. *Nature*, *514*(7522), 355.
789 Jackson, M. G., Shirey, S. B., Hauri, E. H., Kurz, M. D., & Rizo, H. (2016). Peridotite xenoliths
790 from the Polynesian Austral and Samoa hotspots: Implications for the destruction of ancient
791 ^{187}Os and ^{142}Nd isotopic domains and the preservation of Hadean ^{129}Xe in the modern
792 convecting mantle. *Geochimica et Cosmochimica Acta*, *185*, 21-43.
793 Jamais, M., Lassiter, J. C., & Brügmann, G. (2008). PGE and Os-isotopic variations in lavas from
794 Kohala Volcano, Hawaii: constraints on PGE behavior and melt/crust interaction. *Chemical*
795 *Geology*, *250*(1-4), 16-28.
796 Keller, R. A., Fisk, M. R., & White, W. M. (2000). Isotopic evidence for Late Cretaceous plume–
797 ridge interaction at the Hawaiian hotspot. *Nature*, *405*(6787), 673.

798 Konter, J. G., & Jackson, M. G. (2012). Large volumes of rejuvenated volcanism in Samoa:
799 Evidence supporting a tectonic influence on late-stage volcanism. *Geochemistry,*
800 *Geophysics, Geosystems*, *13*(6).
801 Kurz, M. D., Jenkins, W. J., & Hart, S. R. (1982). Helium isotopic systematics of oceanic islands
802 and mantle heterogeneity. *Nature*, *297*(5861), 43-47.
803 Lara, L. E., Díaz-Naveas, J., Reyes, J., Jicha, B., Orozco, G., Tassara, A., & Kay, S. (2018a).
804 Unraveling short-lived rejuvenated volcanism and a rapid transition from shield stage at
805 O'Higgins Guyot, Juan Fernández Ridge, Pacific SE. *Deep Sea Research Part I:*
806 *Oceanographic Research Papers*, *141*, 33-42.
807 Lara, L. E., Reyes, J., & Diaz-Naveas, J. (2018b). $^{40}Ar/^{39}Ar$ constraints on the age progression
808 along the Juan Fernández Ridge, SE Pacific. *Frontiers in Earth Science*, *6*, 194.
809 Lassiter, J. C., Hauri, E. H., Reiners, P. W., & Garcia, M. O. (2000). Generation of Hawaiian post-
810 erosional lavas by melting of a mixed lherzolite/pyroxenite source. *Earth and Planetary*
811 *Science Letters*, *178*(3-4), 269-284.
812 Lassiter, J. C., & Hauri, E. H. (1998). Osmium-isotope variations in Hawaiian lavas: evidence for
813 recycled oceanic lithosphere in the Hawaiian plume. *Earth and Planetary Science*
814 *Letters*, *164*(3), 483-496.
815 Lupton, J. E., & Craig, H. (1975). Excess ^{3}He in oceanic basalts: evidence for terrestrial
816 primordial helium. *Earth and Planetary Science Letters*, *26*(2), 133-139.
817 Maier, W. D., O'Brien, H., Peltonen, P., & Barnes, S. J. (2017). Platinum-group element contents
818 of Karelian kimberlites: Implications for the PGE budget of the sub-continental lithospheric
819 mantle. *Geochimica et Cosmochimica Acta*, *216*, 358-371.

820 Maier, W. D., Peltonen, P., McDonald, I., Barnes, S. J., Barnes, S. J., Hatton, C., & Viljoen, F.
821 (2012). The concentration of platinum-group elements and gold in southern African and
822 Karelian kimberlite-hosted mantle xenoliths: implications for the noble metal content of the
823 Earth's mantle. *Chemical Geology*, *302*, 119-135.
824 McDonough, W. F., & Sun, S. S. (1995). The composition of the Earth. *Chemical geology*, *120*(3-
825 4), 223-253.
826 Meisel, T., Walker, R. J., Irving, A. J., & Lorand, J. P. (2001). Osmium isotopic compositions of
827 mantle xenoliths: a global perspective. *Geochimica et Cosmochimica Acta*, *65*(8), 1311-
828 1323.
829 Mukhopadhyay, S., Lassiter, J. C., Farley, K. A., & Bogue, S. W. (2003). Geochemistry of Kauai
830 shield-stage lavas: Implications for the chemical evolution of the Hawaiian
831 plume. *Geochemistry, Geophysics, Geosystems*, *4*(1).
832 Nagasawa, H., Schreiber, H. D., & Morris, R. V. (1980). Experimental mineral/liquid partition
833 coefficients of the rare earth elements (REE), Sc and Sr for perovskite, spinel and
834 melilite. *Earth and Planetary Science Letters*, *46*(3), 431-437.
835 Natland, J. H. (2003). Capture of helium and other volatiles during the growth of olivine
836 phenocrysts in picritic basalts from the Juan Fernandez Islands. *Journal of Petrology*, *44*(3),
837 421-456.
838 Peters, B. J., & Day, J. M. D. (2014). Assessment of relative Ti, Ta, and Nb (TITAN) enrichments
839 in ocean island basalts. *Geochemistry, Geophysics, Geosystems*, *15*(11), 4424-4444.
840 Peters, B. J., Day, J. M. D., & Taylor, L. A. (2016). Early mantle heterogeneities in the Réunion
841 hotspot source inferred from highly siderophile elements in cumulate xenoliths. *Earth and*
842 *Planetary Science Letters*, *448*, 150-160.

843 Phillips, E. H., Sims, K. W., Sherrod, D. R., Salters, V. J., Blusztajn, J., & Dulai, H. (2016).
844 Isotopic constraints on the genesis and evolution of basanitic lavas at Haleakala, Island of
845 Maui, Hawaii. *Geochimica et Cosmochimica Acta*, *195*, 201-225.
846 Pilet, S., Baker, M. B., & Stolper, E. M. (2008). Metasomatized lithosphere and the origin of
847 alkaline lavas. *Science*, *320*(5878), 916-919.
848 Puchtel, I. S., & Humayun, M. (2001). Platinum group element fractionation in a komatiitic basalt
849 lava lake. *Geochimica et Cosmochimica Acta*, *65*(17), 2979-2993.
850 Regelous, M., Hofmann, A. W., Abouchami, W., & Galer, S. J. G. (2003). Geochemistry of lavas
851 from the Emperor Seamounts, and the geochemical evolution of Hawaiian magmatism from
852 85 to 42 Ma. *Journal of Petrology*, *44*(1), 113-140.
853 Rehkämper, M., Halliday, A. N., Barfod, D., Fitton, J. G., & Dawson, J. B. (1997). Platinum-
854 group element abundance patterns in different mantle environments. *Science*, *278*(5343),
855 1595-1598.
856 Reyes, J., Lara, L. E., & Morata, D. (2017). Contrasting P-T paths of shield and rejuvenated
857 volcanism at Robinson Crusoe Island, Juan Fernández Ridge, SE Pacific. *Journal of*
858 *Volcanology and Geothermal Research, 341, 242-254*.
859 Righter, K., Campbell, A. J., Humayun, M., & Hervig, R. L. (2004). Partitioning of Ru, Rh, Pd,
860 Re, Ir, and Au between Cr-bearing spinel, olivine, pyroxene and silicate melts1. *Geochimica*
861 *et Cosmochimica Acta*, *68*(4), 867-880.
862 Rodrigo, C., & Lara, L. E. (2014). Plate tectonics and the origin of the Juan Fernández Ridge:
863 analysis of bathymetry and magnetic patterns.
864 Roy-Barman, M., & Allègre, C. J. (1995). $^{187}Os/^{186}Os$ in oceanic island basalts: tracing oceanic
865 crust recycling in the mantle. *Earth and Planetary Science Letters*, *129*(1-4), 145-161.

866 Saal, A. E., Kurz, M. D., Hart, S. R., Blusztajn, J. S., Blichert-Toft, J., Liang, Y., & Geist, D. J.
867 (2007). The role of lithospheric gabbros on the composition of Galapagos lavas. *Earth and*
868 *Planetary Science Letters*, *257*(3-4), 391-406.
869 Savard, D., Barnes, S. J., & Meisel, T. (2010). Comparison between nickel-sulfur fire assay Te
870 co-precipitation and isotope dilution with high-pressure asher acid digestion for the
871 determination of platinum-group elements, rhenium and gold. *Geostandards and*
872 *Geoanalytical Research*, *34*(3), 281-291.
873 Selby, D., Creaser, R. A., Stein, H. J., Markey, R. J., & Hannah, J. L. (2007). Assessment of the
874 ^{187}Re decay constant by cross calibration of Re–Os molybdenite and U–Pb zircon
875 chronometers in magmatic ore systems. *Geochimica et Cosmochimica Acta*, *71*(8), 1999-
876 2013.
877 Sen, I. S., Bizimis, M., Sen, G., & Huang, S. (2011). A radiogenic Os component in the oceanic
878 lithosphere? Constraints from Hawaiian pyroxenite xenoliths. *Geochimica et Cosmochimica*
879 *Acta*, *75*(17), 4899-4916.
880 Sinton, J. M., Eason, D. E., & Duncan, R. A. (2017). Volcanic evolution of Moloka ‘i, Hawai ‘i:
881 Implications for the shield to postshield transition in Hawaiian volcanoes. *Journal of*
882 *Volcanology and Geothermal Research*, *340*, 30-51.
883 Sorbadere, F., Médard, E., Laporte, D., & Schiano, P. (2013). Experimental melting of hydrous
884 peridotite–pyroxenite mixed sources: Constraints on the genesis of silica-undersaturated
885 magmas beneath volcanic arcs. *Earth and Planetary Science Letters*, *384*, 42-56.
886 Stuessy, T. F., Foland, K. A., Sutter, J. F., & Silva, M. O. (1984). Botanical and geological
887 significance of potassium-argon dates from the Juan Fernandez Islands. *Science*, *225*, 49-52.

888 Tolstikhin, I., & Hofmann, A. W. (2005). Early crust on top of the Earth's core. *Physics of the*
889 *Earth and Planetary Interiors*, *148*(2-4), 109-130.
890 Truong, T. B., Castillo, P. R., Hilton, D. R., & Day, J. M. D. (2018). The trace element and Sr-Nd-
891 Pb isotope geochemistry of Juan Fernandez lavas reveal variable contributions from a high-
892 $^{3}He/^{4}He$ mantle plume. *Chemical Geology, 476, 280-291*.
893 Valbracht, P. J., Staudacher, T., Malahoff, A., & Allègre, C. J. (1997). Noble gas systematics of
894 deep rift zone glasses from Loihi Seamount, Hawaii. *Earth and Planetary Science*
895 *Letters*, *150*(3-4), 399-411.
896 Weis, D., Garcia, M. O., Rhodes, J. M., Jellinek, M., & Scoates, J. S. (2011). Role of the deep
897 mantle in generating the compositional asymmetry of the Hawaiian mantle plume. *Nature*
898 *Geoscience*, *4*(12), 831.
899 Widom, E., Hoernle, K. A., Shirey, S. B., & Schmincke, H. U. (1999). Os isotope systematics in
900 the Canary Islands and Madeira: lithospheric contamination and mantle plume
901 signatures. *Journal of Petrology*, *40*(2), 279-296.
902 Yang, H. J., Frey, F. A., & Clague, D. A. (2003). Constraints on the source components of lavas
903 forming the Hawaiian North Arch and Honolulu Volcanics. *Journal of Petrology*, *44*(4),
904 603-627.
905

906 **FIGURES AND FIGURE CAPTIONS**

907

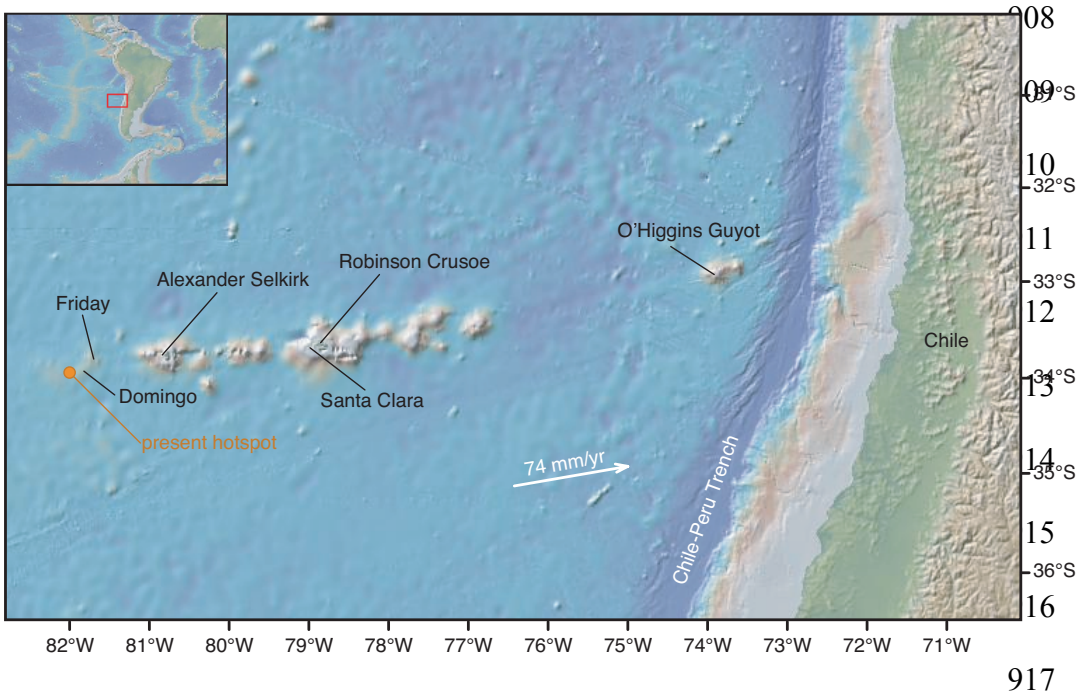

917

918 **Figure 1** – Juan Fernandez Ridge (figure modified from Lara et al., 2018b; map downloaded
919 from www.GeoMapApp.com). The white arrow corresponds to the present day displacement of
920 the Nazca Plate relative to South America (DeMets et al., 2010). O'Higgins Guyot, Santa Clara,
921 Robinson Crusoe Island and Alexander Selkirk Island show $^{40}Ar/^{39}Ar$ ages of 8.41-9.26 Ma,
922 4.58-4.63 Ma, ~3.40-4.10 Ma and ~0.83-0.94 Ma respectively (e.g. Reyes et al., 2017; Lara et
923 al., 2018a, 2018b). The location of the present hotspot is inferred from the age progression
924 defined by Ar ages (Lara et al., 2018b).

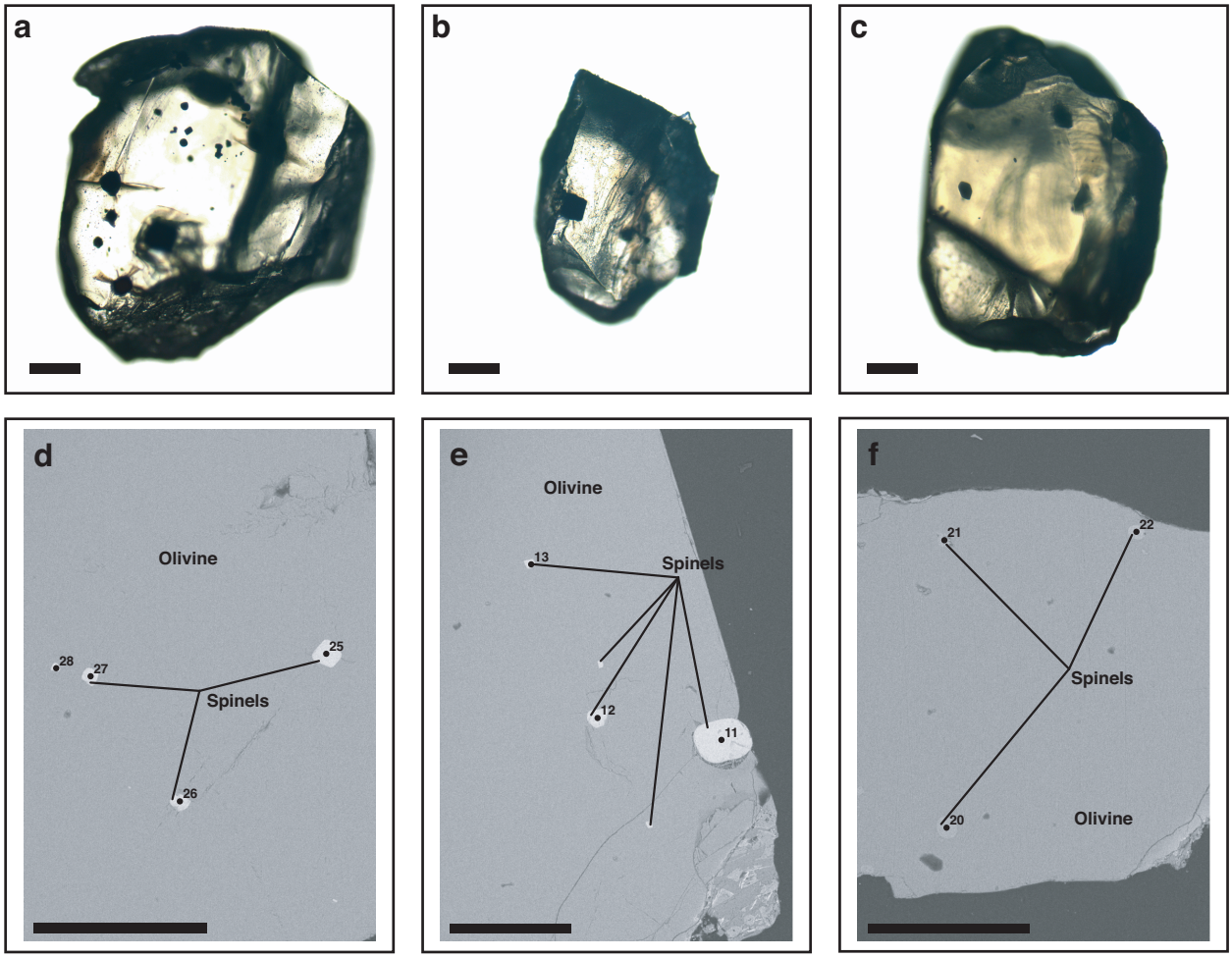

925

926 **Figure 2** - Spinel inclusions in Juan Fernandez olivine grains. (a) PF-5 (Robinson Crusoe main
927 shield lavas), (b) PF-16 (Robinson Crusoe rejuvenated lavas), (c) MF-3 (Alexander Selkirk main
928 shield lavas). Backscattered images of the spinel inclusions in Juan Fernandez olivine grains (d)
929 PF-5 (Robinson Crusoe main shield lavas), (e) PF-16 (Robinson Crusoe rejuvenated lavas), (f)
930 MF-3 (Alexander Selkirk main shield lavas). The scale bar corresponds to 200 µm.

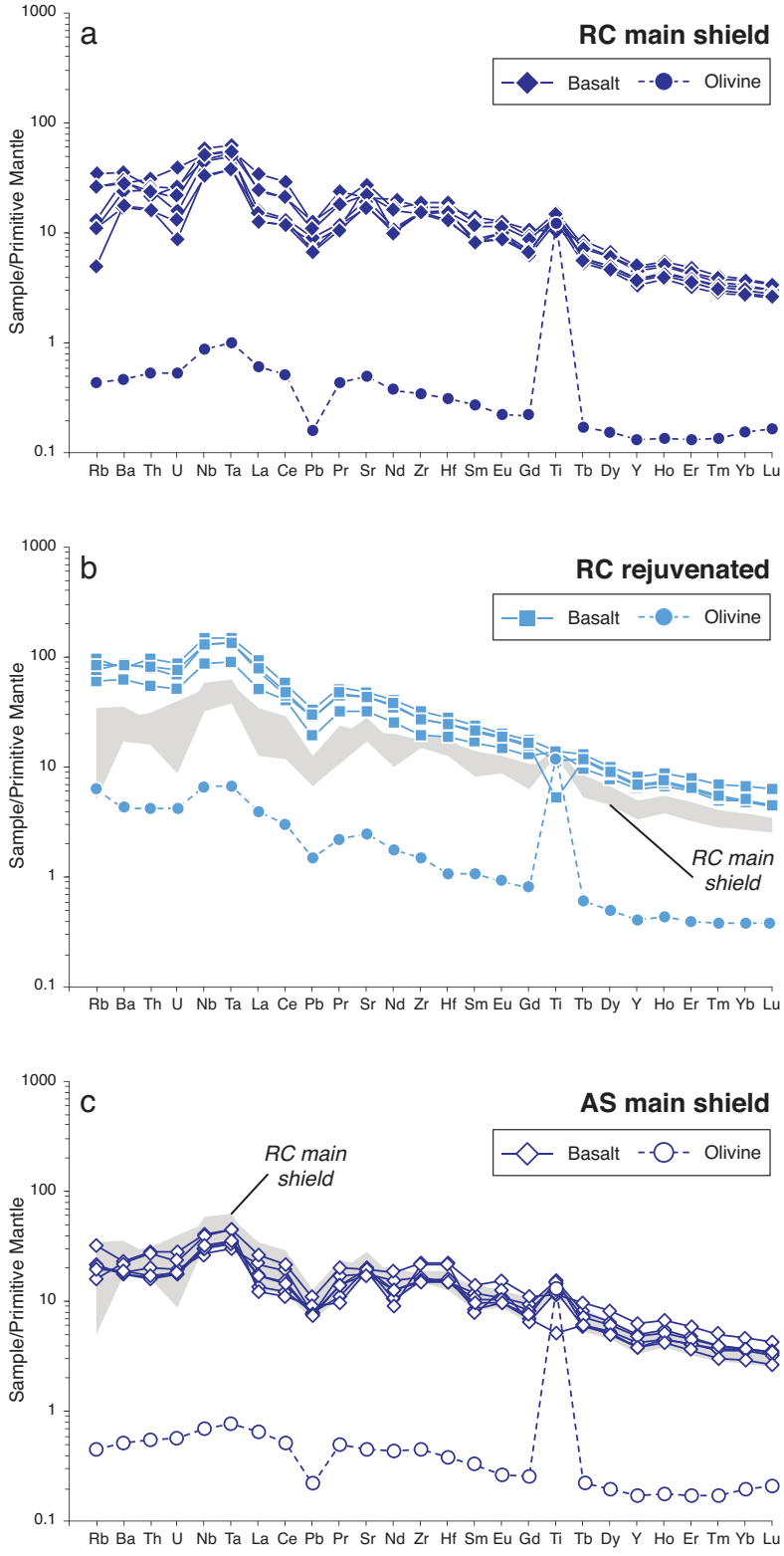

931

932 **Figure 3** – Primitive mantle normalized multi-element variations diagrams for (a) Robinson

933 Crusoe main shield lavas and olivine (black symbols), (b) Robinson Crusoe rejuvenated lavas

934 and olivine (grey symbols), and (c) Alexander Selkirk main shield lavas and olivine (unfilled
935 symbols). Data are normalized to primitive mantle values from McDonough and Sun (1995).
936

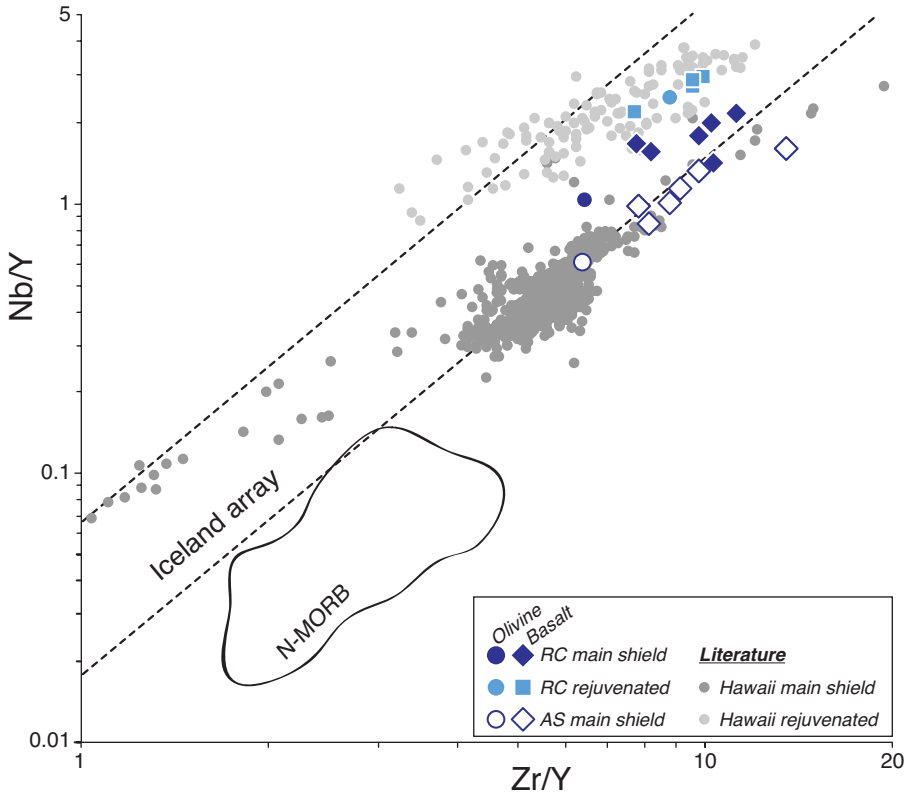

937

938 **Figure 4 -** Niobium/Y versus Zr/Y for Juan Fernandez lavas (diamonds and squares) and
939 olivine grains (circles) compared to Hawaiian rejuvenated (light grey dots) and main shield-stage
940 (dark grey dots) lavas. This diagram discriminates between rejuvenated lavas that form a
941 coherent trend distinct from the main shield lavas (for Juan Fernandez Islands and Hawaii). For
942 the Hawaiian lavas, the offset between these two trends is due to different mantle sources:
943 Hawaiian plume for the main shield lavas and a metasomatized mantle source for the rejuvenated
944 lavas. Various partial melting degrees may also contribute to the vertical offset (e.g. Garcia et al.,

945 2010). RC main shield = Robinson Crusoe main shield lavas and olivine; RC rejuvenated =
946 Robinson Crusoe rejuvenated lavas and olivine; AS main shield = Alexander Selkirk main shield
947 lavas and olivine. Data for Hawaiian main shield stage are from Garcia et al. (1992, 1996, 2000),
948 Mukhopadhyay et al. (2003), Haskins and Garcia (2004), Frey et al. (2016) and references
949 therein, Sinton et al. (2017) and those for the Hawaiian rejuvenated lavas are from Yang et al.
950 (2003), Garcia et al. (2010), Phillips et al. (2016). Diagram after Fitton et al. (1997).
951

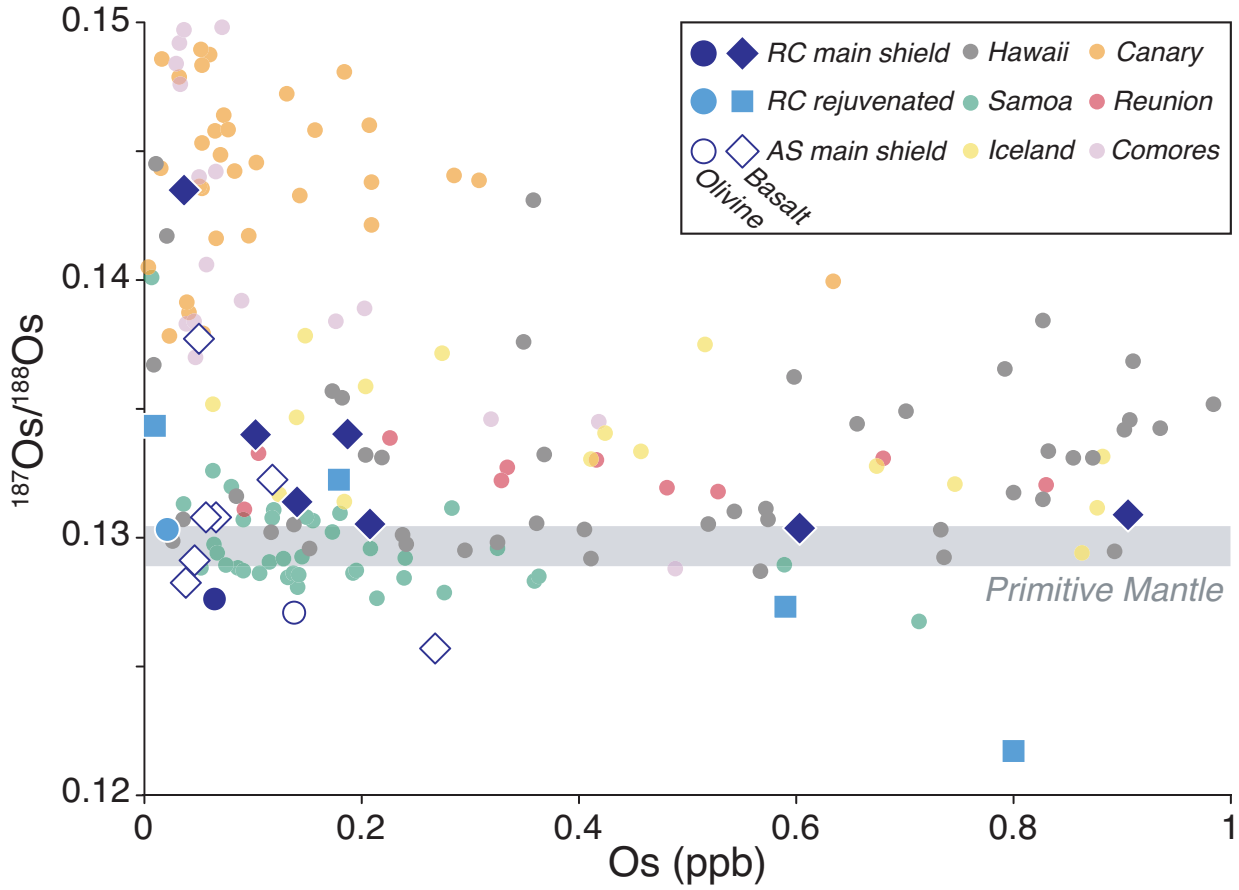

952

953 **Figure 5** – Plot of $^{187}Os/^{188}Os$ ratios versus Os abundances for Juan Fernandez lavas (diamonds
954 and squares) and olivine separates (circles), compared with lavas from Hawaii (Jamais et al.,
955 2008; Ireland et al., 2009), the Comores Islands (Class et al., 2009), Réunion Island (Peters et al.,
956 2016), the Canary Islands (Day et al., 2010), Iceland (Brandon et al., 2007) and Samoa (Jackson

& Shirey, 2011). RC main shield = Robinson Crusoe main shield lavas and olivine; RC rejuvenated = Robinson Crusoe rejuvenated lavas and olivine; AS main shield = Alexander Selkirk main shield lavas and olivine. The grey field represents the primitive mantle range for $^{187}Os/^{188}Os$ from Meisel et al. (2001).

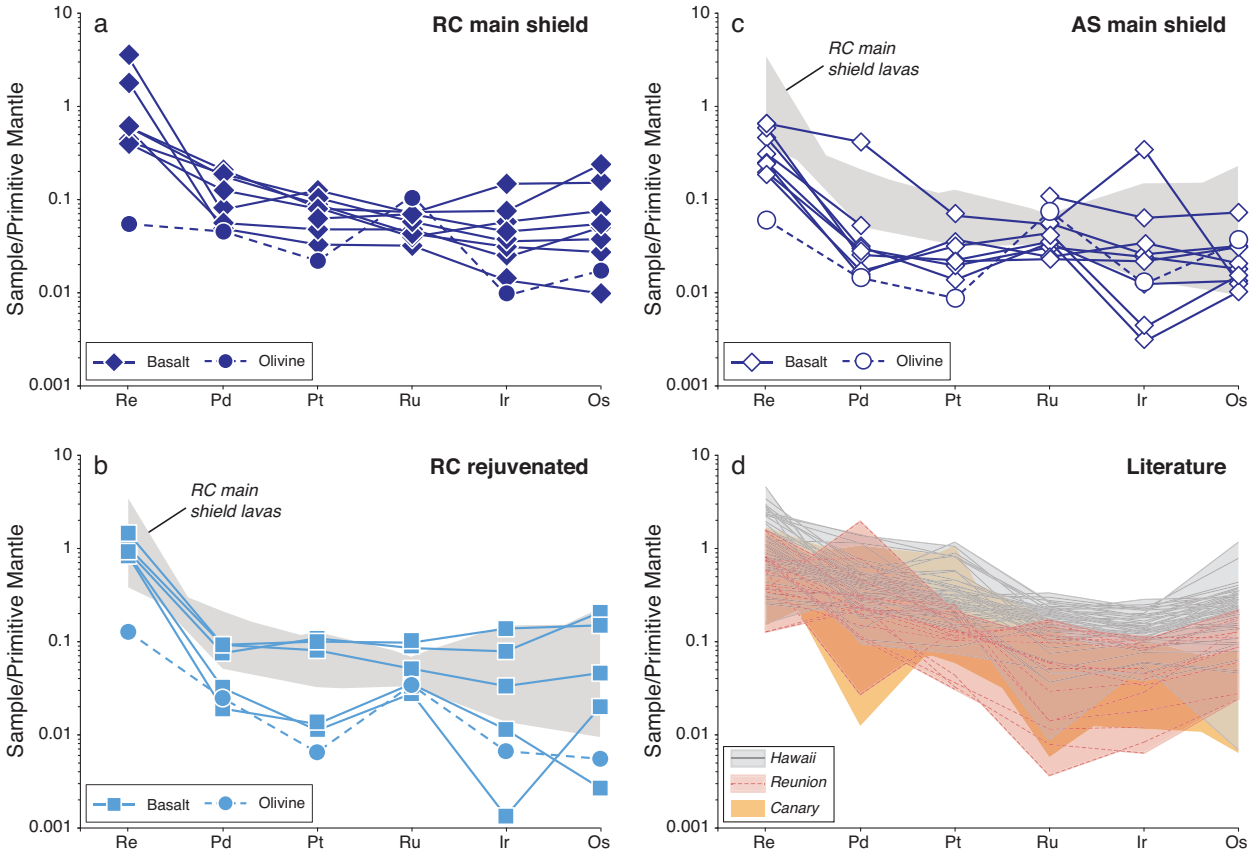

Figure 6 - Highly siderophile elements patterns for Juan Fernandez lavas (diamonds or squares and straight lines) and olivine separates (circles and dashed lines). (a) Robinson Crusoe main shield basalts and olivine; (b) Robinson Crusoe rejuvenated lavas and olivine; (c) Alexander Selkirk main shield lavas and olivine; (d) comparison of lavas from Hawaii (Ireland et al., 2009), the Canary Islands (Day et al., 2010) and Réunion Island (Peters et al., 2016). Data are normalized relative to Primitive Mantle (PM) values from Day et al. (2017).

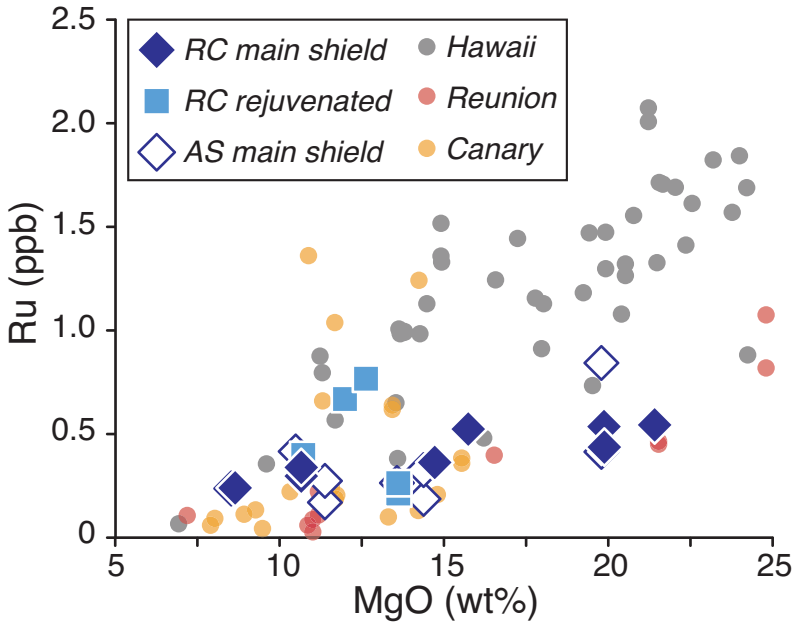

969

970 **Figure 7** - Ruthenium abundances as a function of MgO content for Juan Fernandez lavas
971 (diamonds and squares; olivine grains are not shown), compared with lavas from Hawaii (Ireland
972 et al., 2009), Réunion Island (Peters et al., 2016) and the Canary Islands (Day et al., 2010). RC
973 main shield = Robinson Crusoe main shield lavas; RC rejuvenated = Robinson Crusoe
974 rejuvenated lavas; AS main shield = Alexander Selkirk main shield lavas.

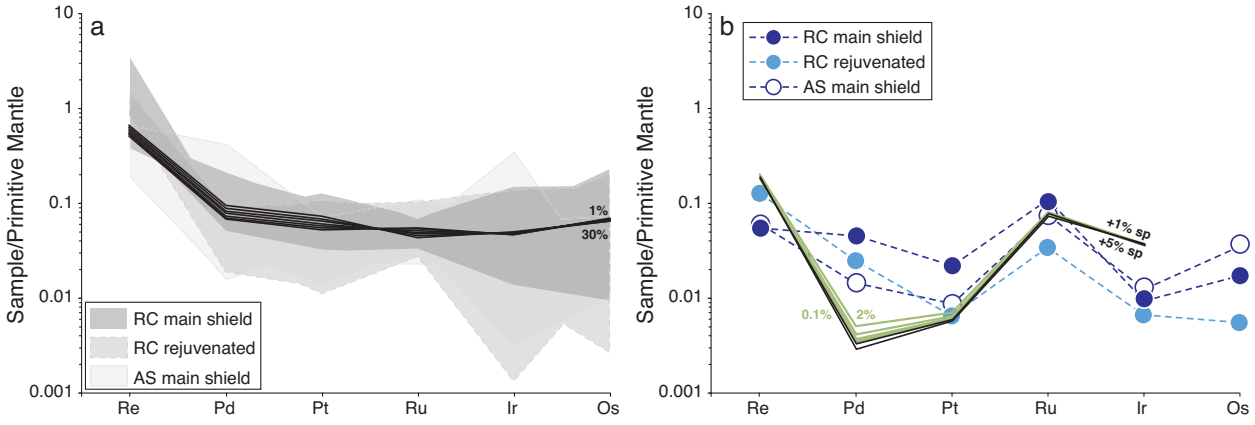

Figure 8 – (a) Modeled compositions of residual melts after fractional crystallization of 1%, 5%, 10%, 15%, 20%, 25% and 30% of olivine (black lines) compared with the compositional ranges of Juan Fernandez lavas (Robinson Crusoe main shield basalts, Robinson Crusoe rejuvenated lavas, and Alexander Selkirk main shield basalts). (b) Composition of olivine after 30% of fractional crystallization from the parent melt of Juan Fernandez lavas, with various amounts of spinel (1% and 5%; black lines) to reproduce the contribution of the spinel inclusions to the HSE composition of olivine separates. The green lines correspond to the composition of the previous mixture of olivine with +5% spinel to which we added the contribution of 0.1% to 2% of the average HSE composition of Juan Fernandez basalts (see Figure 9 for the fractional crystallization modeling of the REE). The parent melt composition was derived from linear regressions of HSE versus MgO trends (see text). The fractionation of 1 to 5% of spinel from the parental melt does not significantly affect the composition of the melt. Partition coefficients for ol/melt and sp/melt are given in the text. Data are normalized relative to Primitive Mantle (PM) values from Day et al. (2017).

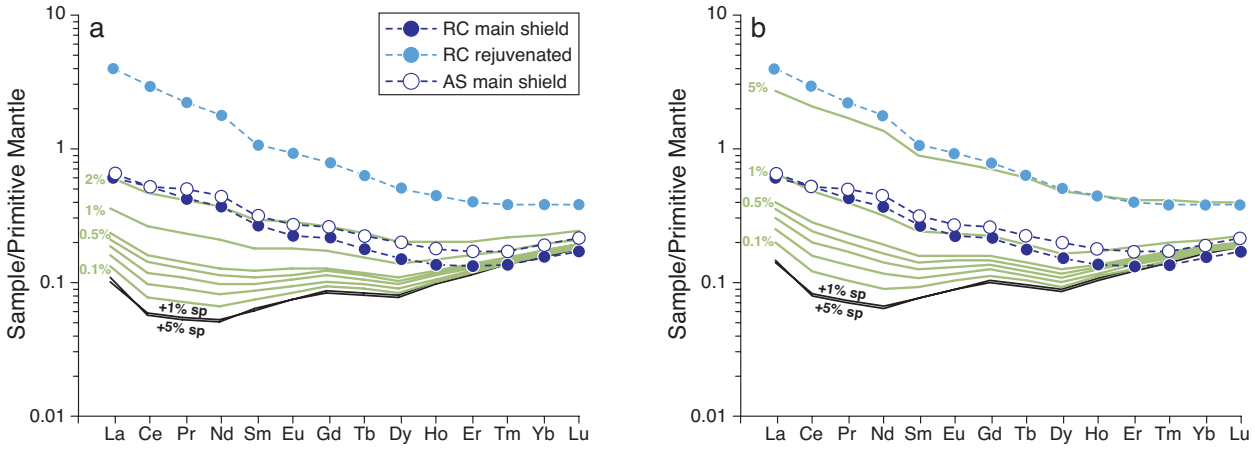

Figure 9 – Composition of olivine after 30% of fractional crystallization from the parent melt of Juan Fernandez lavas, mixed with various amounts of spinel (1% and 5%; black lines) to reproduce the contribution of spinel inclusions to the olivine REE composition. The green lines correspond to the composition of the previous assemblage olivine + 5% spinel, to which we added the contribution of 0.1% to 5% of the composition of the starting material: (a) main shield lava composition, (b) rejuvenated lava composition. Juan Fernandez olivine separates are shown for comparison. As the starting melt composition, we used PF-10 and PF-16, which are the closest to the parent melt composition in terms of MgO content, for Robinson Crusoe main shield and rejuvenated lavas respectively. Partition coefficients for ol/melt are from from Fujimaki et al. (1984), and those for sp/melt from Nagasawa et al. (1980). Data are normalized relative to Primitive Mantle (PM) values from McDonough & Sun (1995).

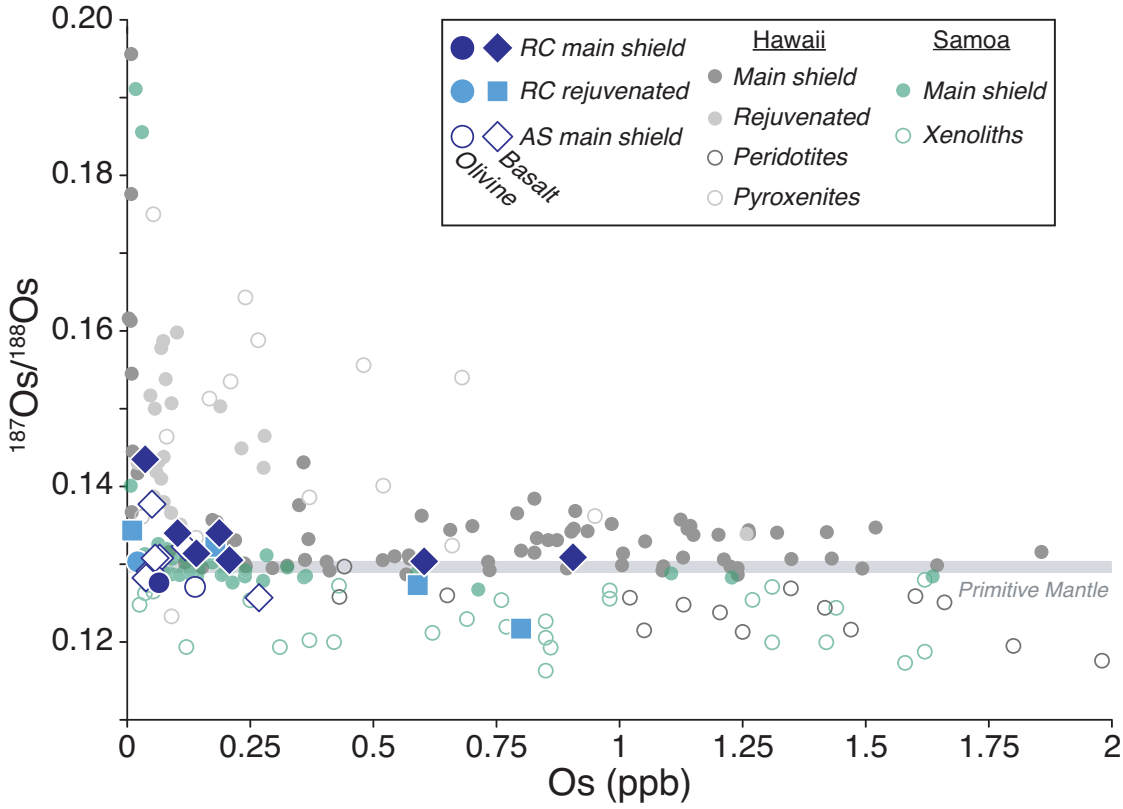

1008

1009 **Figure 10** – Plot of $^{187}Os/^{188}Os$ ratios versus Os abundances for Juan Fernandez lavas (diamonds
1010 and squares) and olivine separates (circles), compared with main shield lavas (Hawaii: Jamais et
1011 al., 2008; Ireland et al., 2009; Samoa: Jackson & Shirey, 2011), rejuvenated lavas (Hawaii:
1012 Lassiter et al., 2000; Samoa: Konter and Jackson, 2012), xenoliths (Hawaii: peridotites from
1013 Lassiter et al., 2000: Bizimis et al., 2007; pyroxenites from Lassiter et al., 2000; Sen et al., 2011;
1014 Samoa: Jackson et al., 2016). RC main shield = Robinson Crusoe main shield lavas and olivine;
1015 RC rejuvenated = Robinson Crusoe rejuvenated lavas and olivine; AS main shield = Alexander
1016 Selkirk main shield lavas and olivine. The grey field represents the primitive mantle range for
1017 $^{187}Os/^{188}Os$ from Meisel et al. (2001).

1018

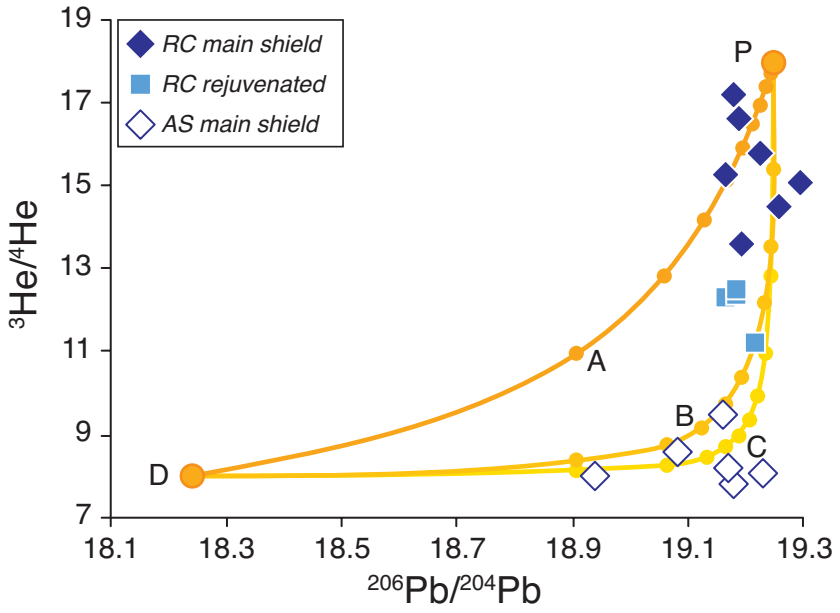

1019

1020 **Figure 11** – Plot of He versus Pb isotope variation for Juan Fernandez samples illustrating
1021 binary mixing trajectories between depleted component (D) and a high-^{3}He hotspot endmember
1022 (P). Isotopic values for D are from Hilton et al. (2000). The He isotope characteristics of P is
1023 taken as $18R_A$, as the highest ratio measured for Robinson Crusoe main shield lavas (Farley et
1024 al., 1993). The plume lead isotopic composition $^{206}Pb/^{204}Pb$ is taken as 19.25 in order to be
1025 slightly higher than the average isotopic composition for Robinson Crusoe main shield lavas.
1026 Curves are labeled to represent the mixing with variably degassed plume sources: (A)
1027 undegassed mantle plume ^{4}He abundance is taken as 56 µcm^{3}STP/g, which is the ^{4}He content in
1028 PIN-8 and the value for the undegassed mantle used by Hilton et al., 2000), (B) and (C) represent
1029 depletions of x12 and x36, respectively, relative to the initial plume He content. Dots along the
1030 mixing curves represent a 10% increment in the mixing proportions between the two
1031 endmembers. RC main shield = Robinson Crusoe main shield lavas; RC rejuvenated = Robinson
1032 Crusoe rejuvenated lavas; AS main shield = Alexander Selkirk main shield lavas.

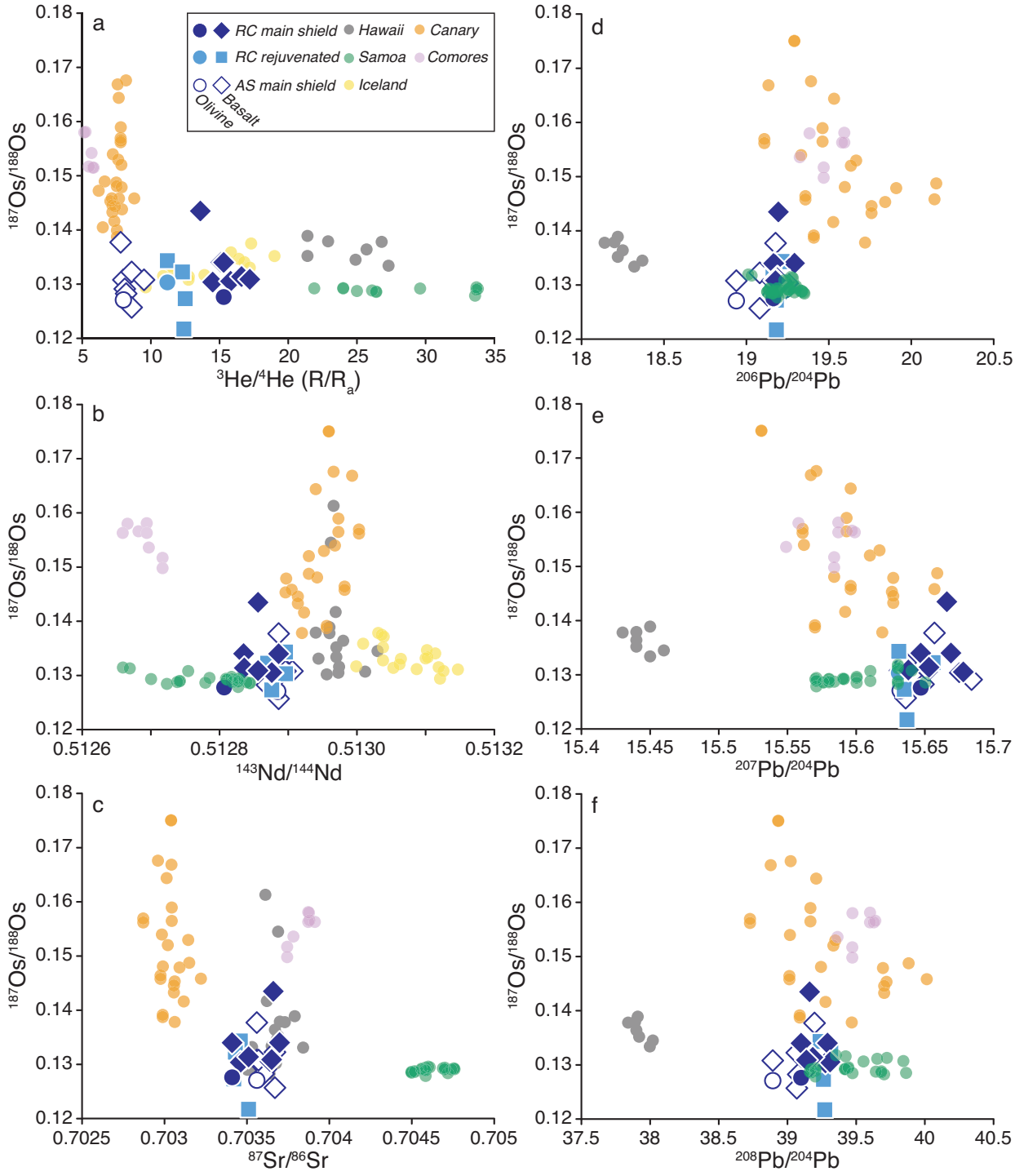

Figure 12 – Osmium isotope compositions compared with (a) $^{3}He/^{4}He$ (R/R_a), (b) $^{143}Nd/^{144}Nd$, (c) $^{87}Sr/^{86}Sr$, (d) $^{206}Pb/^{204}Pb$, (e) $^{207}Pb/^{204}Pb$ and (f) $^{208}Pb/^{204}Pb$ for Juan Fernandez lavas (diamonds and squares) and olivine separates (circles), and compared with lavas from Hawaii

1037 (Mukhopadhyay et al., 2003; Bryce et al., 2005; Jamais et al., 2008), the Comores Islands (Class
1038 et al., 1998, 2005, 2009), the Canary Islands (Day et al., 2010, Day & Hilton, 2011), Iceland
1039 (Brandon et al., 2007;) and Samoa (Jackson et al., 2007, Jackson & Shirey, 2011; Konter and
1040 Jackson, 2012). RC main shield = Robinson Crusoe main shield lavas and olivine; RC
1041 rejuvenated = Robinson Crusoe rejuvenated lavas and olivine; AS main shield = Alexander
1042 Selkirk main shield lavas and olivine.
1043

SUPPLEMENTARY INFORMATION

Supplementary Discussion

a. Data comparison

A comparison of the trace element abundances for Juan Fernandez lavas obtained on unleached powders in this study using a *Thermo Fisher Scientific* iCAP Qc ICP-MS and those reported by Truong et al. (2018) using a *ThermoQuest* Element 2 ICP-MS is presented in Figure S1. Overall, our analyses for Juan Fernandez lavas are in good agreement with the measurements published by Truong et al. (2018) and Farley et al. (1993). We report slightly lower abundances of Zr than Truong et al. (2018). This could be due to unaccounted-for interferences of Ar and Ti or Cr on ^{90}Zr in the study of Troung et al. (2018). In this study, we report new data for the following elements: Sc, V, Cr, Co Ni, Cu, Zn, Rb, Ba, Nb, Sr, Zr, Y, La, Ce Pr, Nd, Sm, Eu, Gd, Tb, Dy, Ho, Er Tm, Yb, Lu, Hf, Ta, Pb, Th, U, Ga, Ge, Se, Mo, Sn, Te and W. In particular, Sc, Gd, Tm, Ge, Se, Mo, Sn, Te and W are measured for the first time in Juan Fernandez lavas and olivine separates.

b. Fe-Mn oxide contamination

Iron-Mn oxide coatings have been suggested as potential contaminants during OIB petrogenesis (e.g., Ireland et al., 2009a). They are characterized by radiogenic ^{187}Os/^{188}Os compositions and high Os abundances. These materials tend to incorporate the HSE from seawater, in particular Pt (e.g., Ireland et al., 2009a and references therein). Sample MF-S1 contains a high concentration of Pt, which could be due to pervasive alteration by Mn-rich material as described by Ireland et al. (2009a) in a sample from Koolau in Hawaii. However, the

1067 Fe-Mn oxide assimilation process is expected to change the MnO content of the melt. There is no
1068 indication of Mn enrichment for sample MF-S1 (MnO = 0.17 wt.%; Farley et al., 1993). Instead,
1069 this Pt enrichment may be due to contamination during sample preparation and prior to analysis.
1070
1071 ***c. Magmatic degassing of rhenium***
1072 During mantle partial melting and fractional crystallization, La and Yb are incompatible,
1073 while Re behaves similarly to Yb (Hauri and Hart, 1997; Bennett et al., 2000; Norman et al.,
1074 2004). Additionally, Re, Os and Cu abundances are controlled by residual sulfide and are
1075 expected to behave coherently during melting (Bennett et al., 2000). There is a relationship of
1076 decreasing Re/Os, Re/Yb and Re/Cu with decreasing Re abundance for the Juan Fernandez lavas
1077 (Figure S7). Such a relationship is not observed for Cu/Yb, La/Yb or Os/Yb with decreasing Re
1078 abundances. These characteristics suggest Re loss during magmatic degassing (c.f. Day et al.,
1079 2010). Nevertheless, it is unlikely that the other HSE experience such significant volatile
1080 behavior, as the ratios of these elements versus Yb remain constant or even increase slightly with
1081 decreasing Re content (Figure S7), and they correlate positively with indices of magmatic
1082 differentiation, such as MgO (Figures 7 and S4).
1083
1084 **d. Ingrowth of radiogenic osmium**
1085 The samples that we analyzed from the Juan Fernandez Islands are all >1 Ma, offering
1086 potential for ingrowth of radiogenic Os from ^{187}Re decay. The samples have low $^{187}Re/^{188}Os$
1087 (<10), however, precluding significant ingrowth (Figure S8) and these are corrected for in Table
1088 1.
1089

Supplementary References

Bennett, V. C., Norman, M. D., & Garcia, M. O. (2000). Rhenium and platinum group element abundances correlated with mantle source components in Hawaiian picrites: sulphides in the plume. *Earth and Planetary Science Letters*, *183*(3), 513-526.

Bizimis, M., Griselin, M., Lassiter, J. C., Salters, V. J., & Sen, G. (2007). Ancient recycled mantle lithosphere in the Hawaiian plume: osmium–hafnium isotopic evidence from peridotite mantle xenoliths. *Earth and Planetary Science Letters*, *257*(1-2), 259-273.

Bryce, J. G., DePaolo, D. J., & Lassiter, J. C. (2005). Geochemical structure of the Hawaiian plume: Sr, Nd, and Os isotopes in the 2.8 km HSDP‐2 section of Mauna Kea volcano. *Geochemistry, Geophysics, Geosystems*, *6*(9).

Day, J. M. D., Pearson, D. G., Macpherson, C. G., Lowry, D., & Carracedo, J. C. (2010). Evidence for distinct proportions of subducted oceanic crust and lithosphere in HIMU-type mantle beneath El Hierro and La Palma, Canary Islands. *Geochimica et Cosmochimica Acta*, *74*(22), 6565-6589.

Debaille, V., Trønnes, R. G., Brandon, A. D., Waight, T. E., Graham, D. W., & Lee, C. T. A. (2009). Primitive off-rift basalts from Iceland and Jan Mayen: Os-isotopic evidence for a mantle source containing enriched subcontinental lithosphere. *Geochimica et Cosmochimica Acta*, *73*(11), 3423-3449.

Farley, K. A., Basu, A. R., & Craig, H. (1993). He, Sr and Nd isotopic variations in lavas from the Juan Fernandez Archipelago, SE Pacific. *Contributions to Mineralogy and Petrology*, *115*(1), 75-87.

Hauri, E. H., & Hart, S. R. (1997). Rhenium abundances and systematics in oceanic basalts. *Chemical Geology*, *139*(1), 185-205.

1113 Ireland, T. J., Walker, R. J., & Garcia, M. O. (2009a). Highly siderophile element and ^{187}Os
1114 isotope systematics of Hawaiian picrites: implications for parental melt composition and
1115 source heterogeneity. *Chemical Geology*, *260*(1), 112-128.
1116 Ireland, T. J., Arevalo, R., Walker, R. J., & McDonough, W. F. (2009b). Tungsten in Hawaiian
1117 picrites: A compositional model for the sources of Hawaiian lavas. *Geochimica et*
1118 *Cosmochimica Acta*, *73*(15), 4517-4530.
1119 Jackson, M. G., & Shirey, S. B. (2011). Re–Os isotope systematics in Samoan shield lavas and the
1120 use of Os-isotopes in olivine phenocrysts to determine primary magmatic
1121 compositions. *Earth and Planetary Science Letters*, *312*(1), 91-101.
1122 Jackson, M. G., Kurz, M. D., Hart, S. R., & Workman, R. K. (2007). New Samoan lavas from Ofu
1123 Island reveal a hemispherically heterogeneous high 3 He/4 He mantle. *Earth and Planetary*
1124 *Science Letters*, *264*(3), 360-374.
1125 Jamais, M., Lassiter, J. C., & Brügmann, G. (2008). PGE and Os-isotopic variations in lavas from
1126 Kohala Volcano, Hawaii: constraints on PGE behavior and melt/crust interaction. *Chemical*
1127 *Geology*, *250*(1-4), 16-28.
1128 Konter, J. G., & Jackson, M. G. (2012). Large volumes of rejuvenated volcanism in Samoa:
1129 Evidence supporting a tectonic influence on late‐stage volcanism. *Geochemistry,*
1130 *Geophysics, Geosystems*, *13*(6).
1131 Lassiter, J. C., Hauri, E. H., Reiners, P. W., & Garcia, M. O. (2000). Generation of Hawaiian post-
1132 erosional lavas by melting of a mixed lherzolite/pyroxenite source. *Earth and Planetary*
1133 *Science Letters*, *178*(3-4), 269-284.

1134 Meisel, T., Walker, R. J., Irving, A. J., & Lorand, J. P. (2001). Osmium isotopic compositions of
1135 mantle xenoliths: a global perspective. *Geochimica et Cosmochimica Acta*, *65*(8), 1311-
1136 1323.
1137 McDonough, W. F., & Sun, S. S. (1995). The composition of the Earth. *Chemical geology*, *120*(3-
1138 4), 223-253.
1139 Mukhopadhyay, S., Lassiter, J. C., Farley, K. A., & Bogue, S. W. (2003). Geochemistry of Kauai
1140 shield-stage lavas: Implications for the chemical evolution of the Hawaiian
1141 plume. *Geochemistry, Geophysics, Geosystems*, *4*(1).
1142 Norman, M. D., Garcia, M. O., & Bennett, V. C. (2004). Rhenium and chalcophile elements in
1143 basaltic glasses from Ko'olau and Moloka'i volcanoes: Magmatic outgassing and
1144 composition of the Hawaiian plume. *Geochimica et Cosmochimica Acta*, *68*(18), 3761-3777.
1145 Peters, B. J., Day, J. M. D., & Taylor, L. A. (2016). Early mantle heterogeneities in the Réunion
1146 hotspot source inferred from highly siderophile elements in cumulate xenoliths. *Earth and*
1147 *Planetary Science Letters*, *448*, 150-160.
1148 Sen, I. S., Bizimis, M., Sen, G., & Huang, S. (2011). A radiogenic Os component in the oceanic
1149 lithosphere? Constraints from Hawaiian pyroxenite xenoliths. *Geochimica et Cosmochimica*
1150 *Acta*, *75*(17), 4899-4916.
1151 Truong, T. B., Castillo, P. R., Hilton, D. R., & Day, J. M. D. (2018). The trace element and Sr-Nd-
1152 Pb isotope geochemistry of Juan Fernandez lavas reveal variable contributions from a high-
1153 $^{3}He/^{4}He$ mantle plume. *Chemical Geology, 476, 280-291*.
1154

SUPPLEMENTARY FIGURES AND CAPTIONS

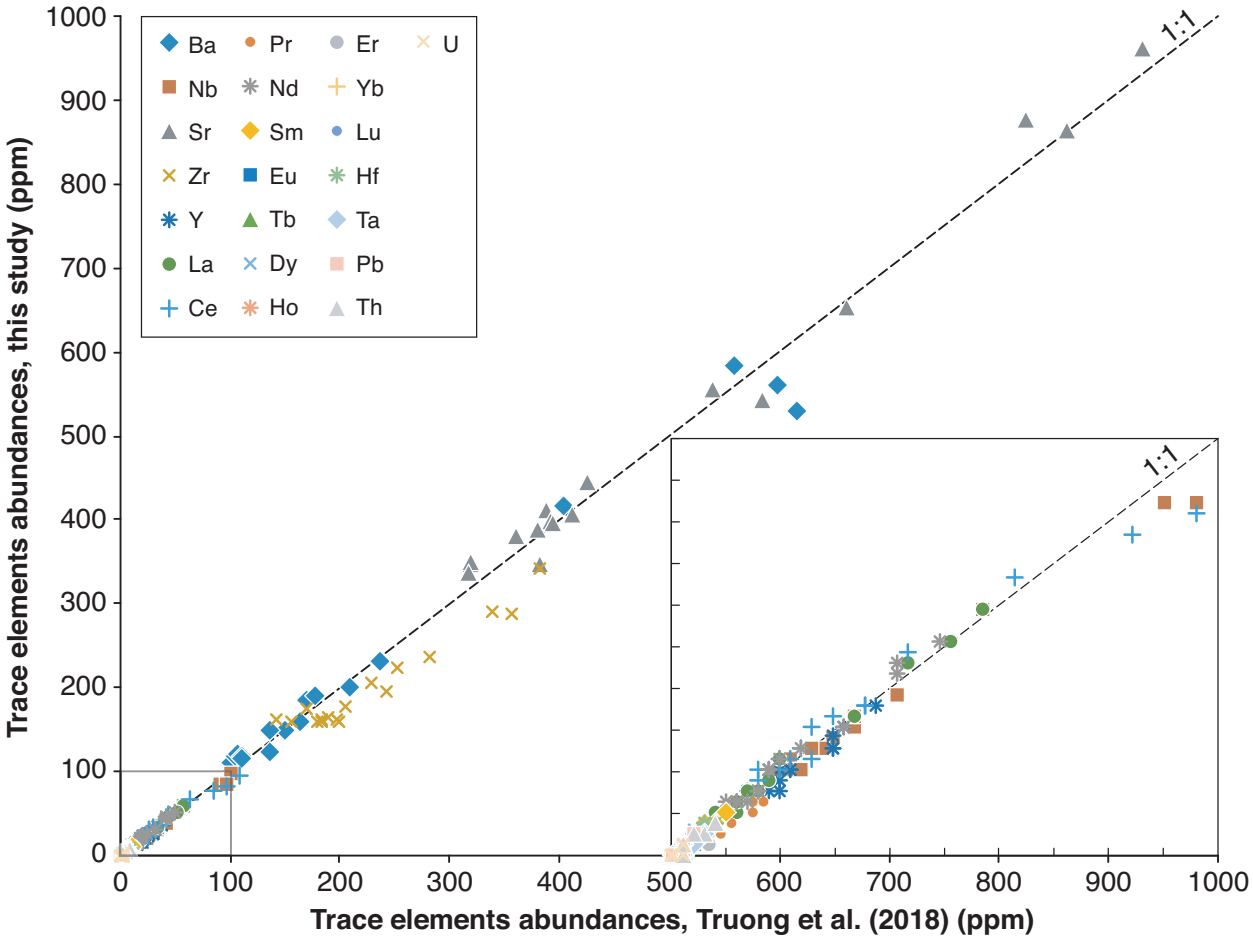

Figure S1 – Comparison of the trace element abundances for Juan Fernandez lavas obtained in this study (*Thermo Fisher Scientific* iCaP Qc ICP-MS) versus those reported by Truong et al. (2018) (*ThermoQuest Element* 2 ICP-MS). Both studies were conducted on unleached powders due to the low degree of alteration visible in samples.

1161

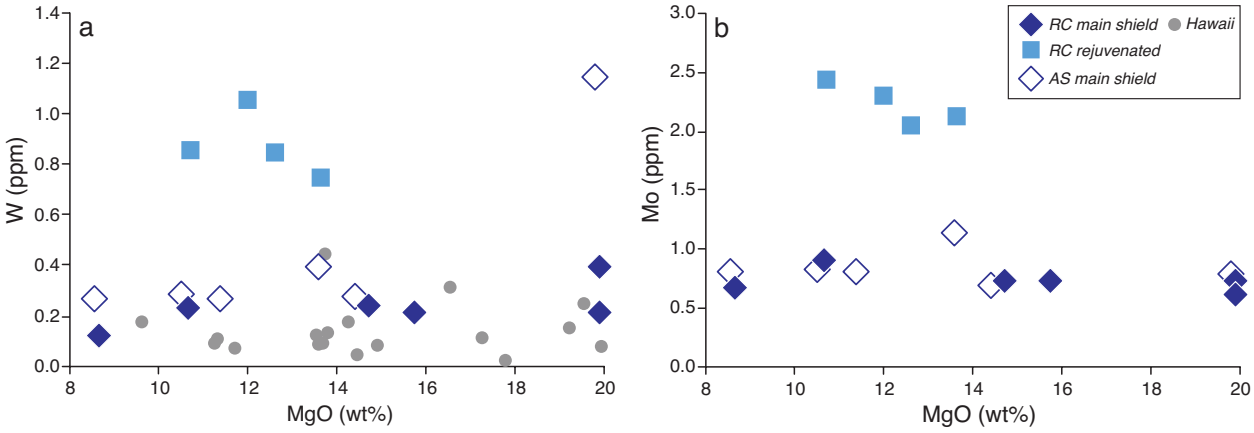

1162

1163 **Figure S2** – (a) W and (b) Mo abundances versus MgO content for Juan Fernandez lavas

1164 (olivine separates are not represented), compared with lavas from Hawaii (Ireland et al., 2009b).

1165

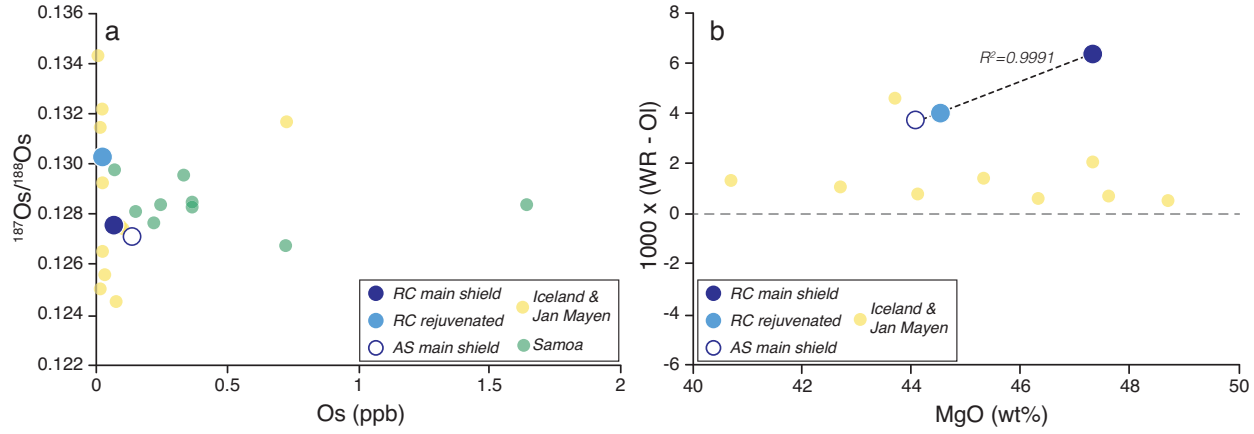

1166

1167 **Figure S3** – (a) Osmium abundances versus $^{187}Os/^{188}Os$ in Juan Fernandez olivine separates,

1168 compared with olivines from Samoa (Jackson and Shirey, 2011) and Iceland and Jan Mayen

1169 (Debaille et al., 2009). (b) Magnesium content versus $^{187}Os/^{188}Os$ between basalt hosts and

1170 olivine separates. R-squared values are from linear regression. RC main shield = Robinson

1171 Crusoe main shield olivine; RC rejuvenated = Robinson Crusoe rejuvenated olivine; AS main

1172 shield = Alexander Selkirk main shield olivine.

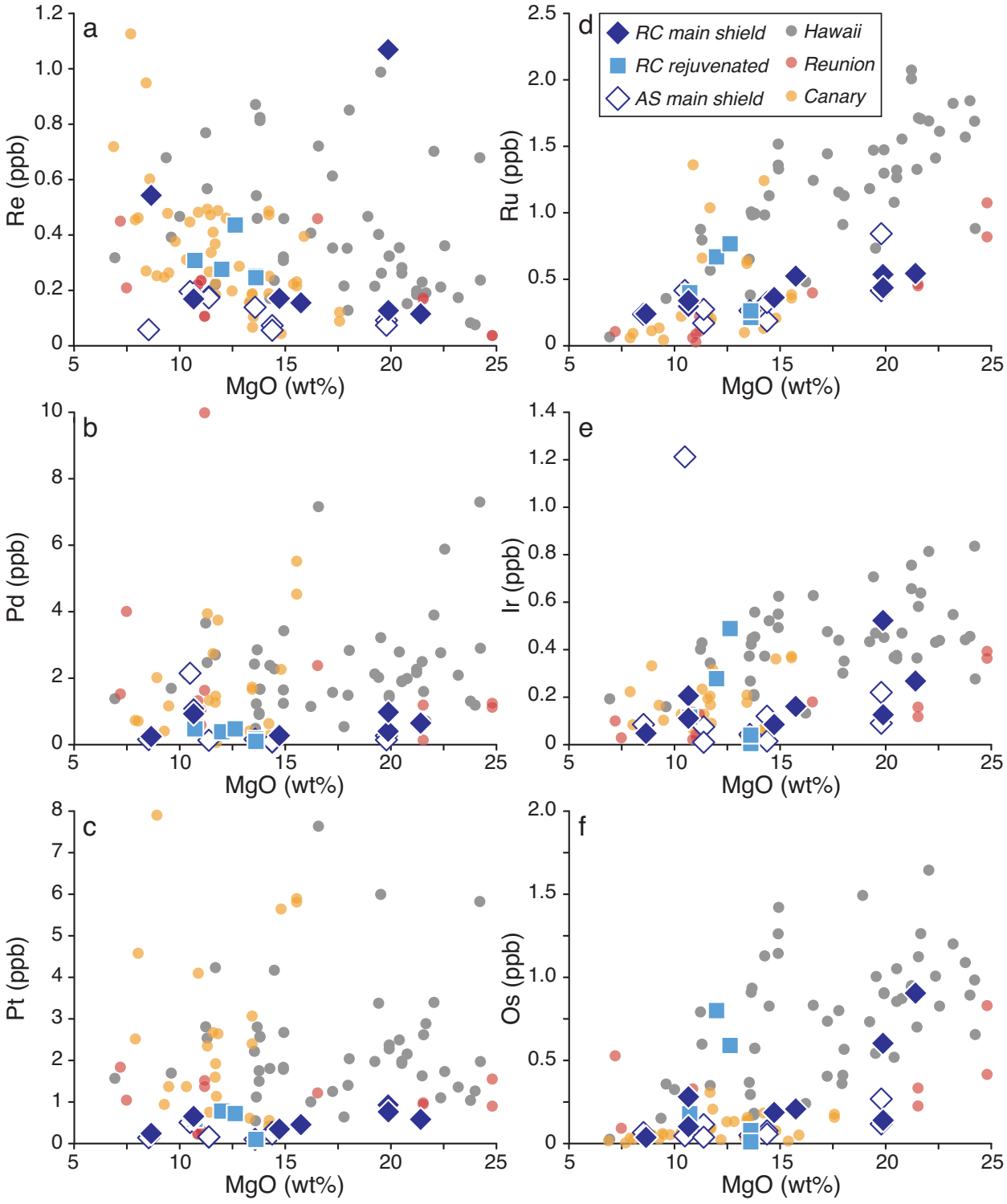

Figure S4 – Juan Fernandez lavas HSE-MgO trends (diamonds and squares; olivine separates are not shown), compared with lavas from Hawaii (Ireland et al., 2009a), Réunion Island (Peters et al., 2016), and the Canary Islands (Day et al., 2010). RC main shield = Robinson Crusoe main

shield lavas; RC rejuvenated = Robinson Crusoe rejuvenated lavas; AS main shield = Alexander Selkirk main shield lavas.

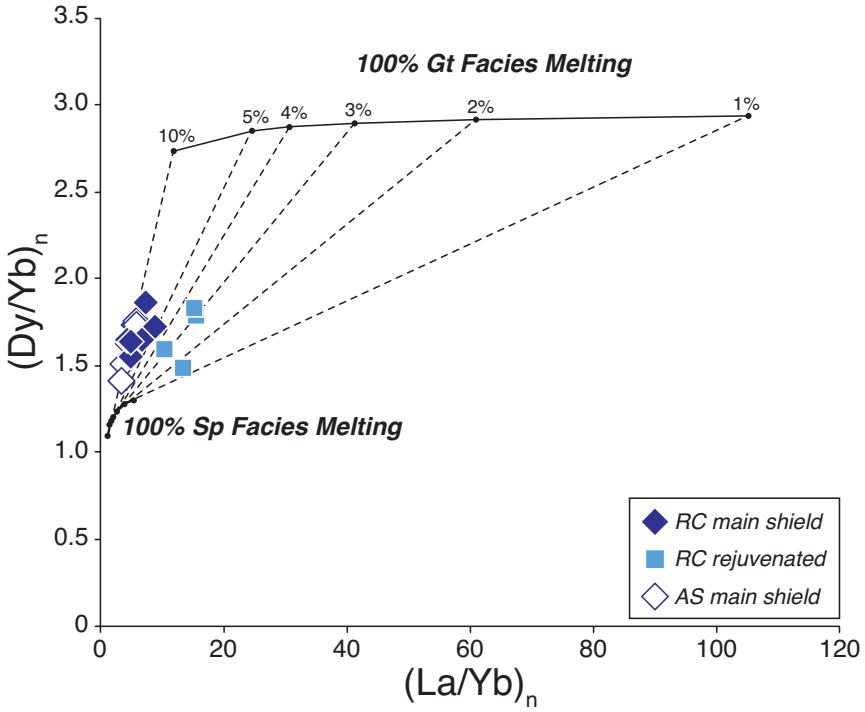

Figure S5 – $(La/Yb)_n$ versus $(Dy/Yb)_n$ for Juan Fernandez lavas. Ratios are normalized to CI-chondrites from McDonough and Sun (1995). The incremental partial melting model is calculated with parameters from Day et al. (2010; Table S6), assuming a primitive mantle source (garnet peridotite with modal proportions of olivine, orthopyroxene, clinopyroxene and garnet of 0.54/0.17/0.09/0.20; spinel peridotite with modal proportions of olivine, orthopyroxene, clinopyroxene and spinel of 0.54/0.17/0.09/0.20).

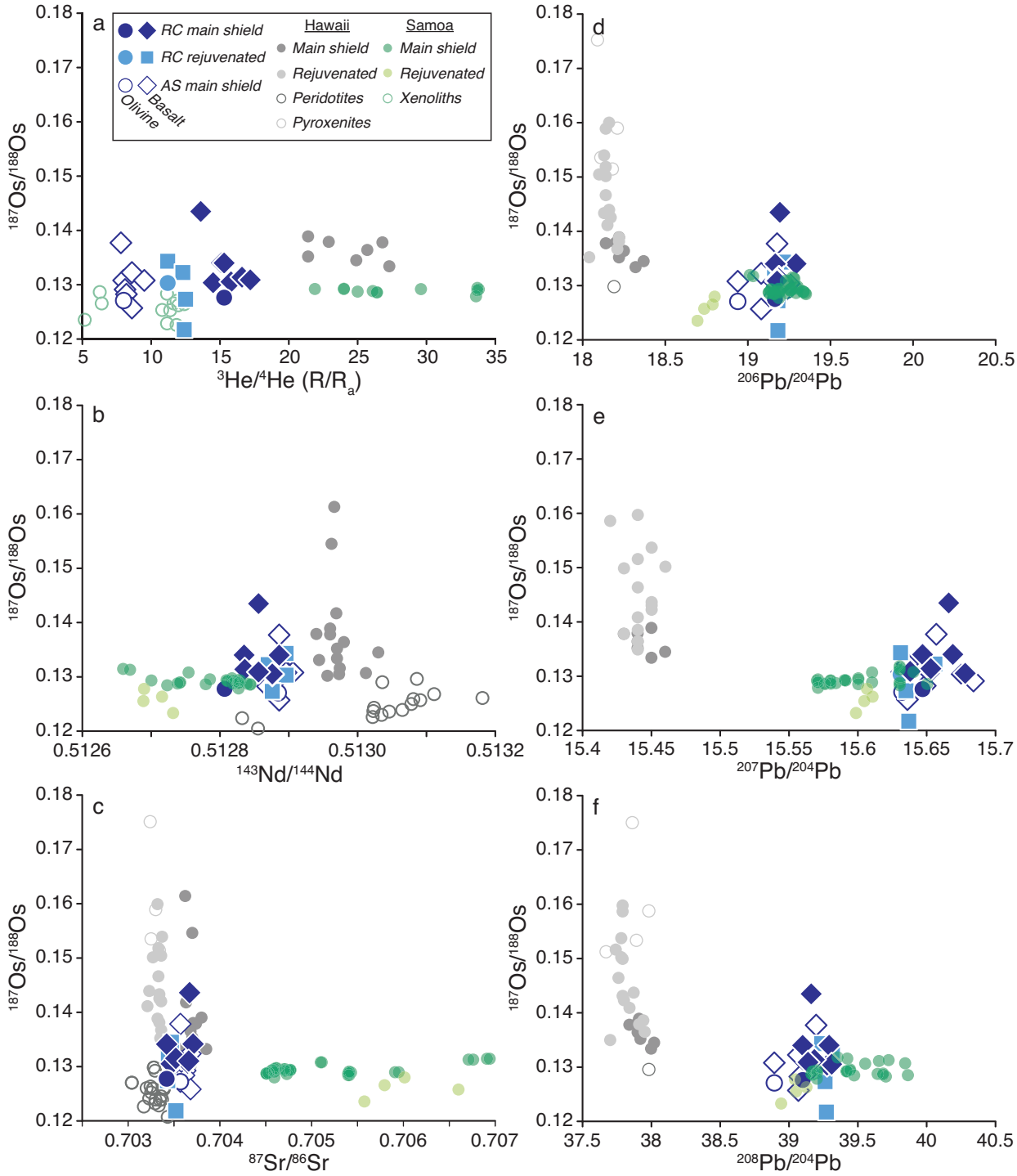

Figure S6 – Osmium isotope compositions compared with (a) $^{3}He/^{4}He$ (R/R_a), (b) $^{143}Nd/^{144}Nd$, (c) $^{87}Sr/^{86}Sr$, (d) $^{206}Pb/^{204}Pb$, (e) $^{207}Pb/^{204}Pb$ and (f) $^{208}Pb/^{204}Pb$ for Juan Fernandez lavas (diamonds and squares) and olivine separates (circles), and compared with main shield lavas (Hawaii: Mukhopadhyay et al., 2003; Bryce et al., 2005; Jamais et al., 2008; Samoa Jackson et

al., 2007, Jackson & Shirey, 2011; Konter and Jackson, 2012), rejuvenated lavas (Hawaii: Lassiter et al., 2000; Samoa: Konter and Jackson, 2012), xenoliths (Hawaii: peridotites from Lassiter et al., 2000: Bizimis et al., 2007; pyroxenites from Lassiter et al., 2000; Sen et al., 2011; Samoa: Jackson et al., 2016). RC main shield = Robinson Crusoe main shield lavas and olivine; RC rejuvenated = Robinson Crusoe rejuvenated lavas and olivine; AS main shield = Alexander Selkirk main shield lavas and olivine.

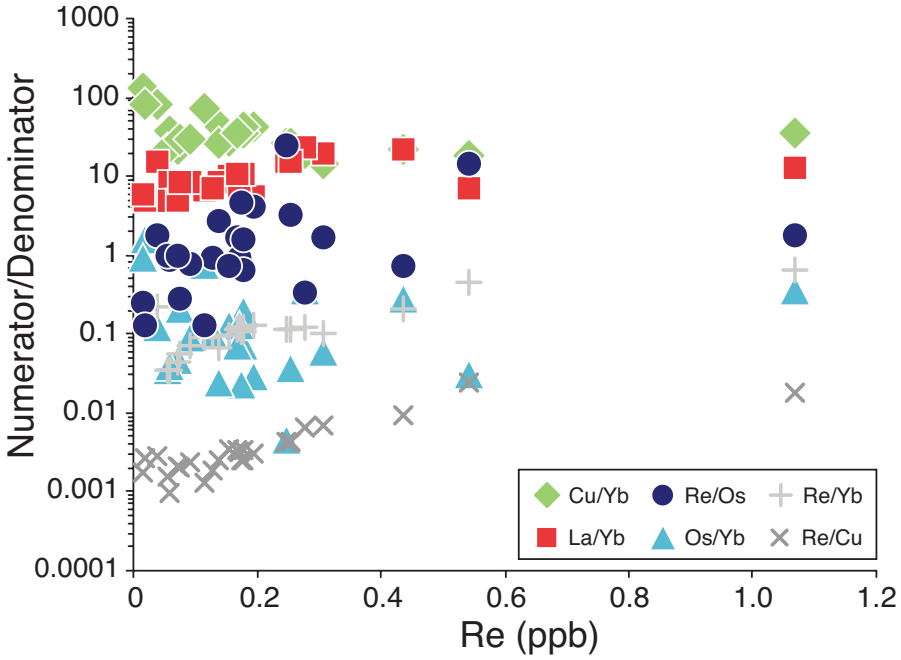

Figure S7 – Ratios of (La, Cu, Os, Re)/Yb, Re/Cu and Re/Os for Juan Fernandez lavas and olivine grains, to assess potential magmatic degassing of rhenium.

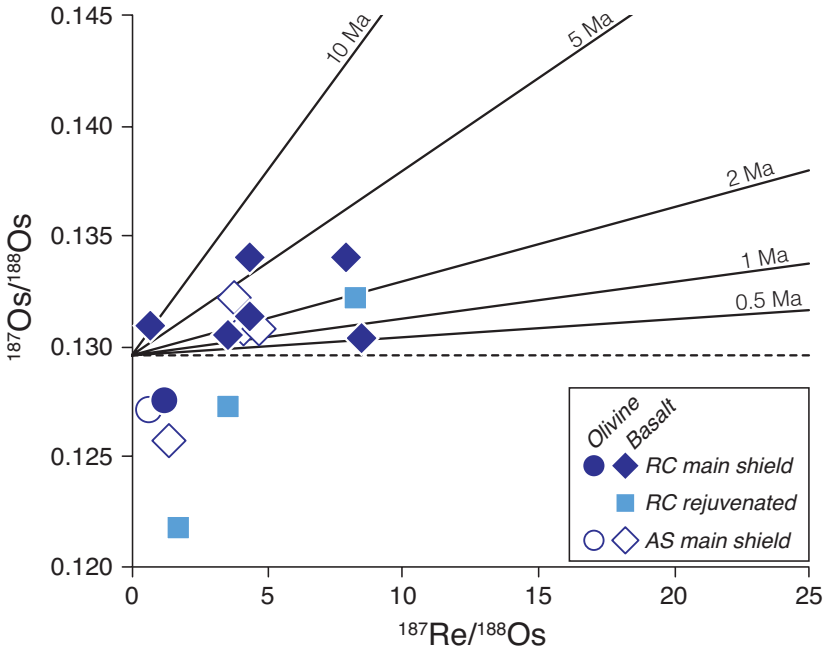

1202

1203 **Figure S8** – $^{187}Os/^{188}Os$ ratios versus $^{187}Re/^{188}Os$ ratios for Juan Fernandez lavas and olivine
1204 grains with Os abundances > 50 ppt. There is no clear correlation with $^{187}Re/^{188}Os$ and
1205 $^{187}Os/^{188}Os$ in the Juan Fernandez Islands dataset. The $^{187}Os/^{188}Os$ ratio for the primitive mantle
1206 is from Meisel et al. (2001).

1207